Title: Intracellular pH-regulated Cell Intrinsic Control of Death and Proliferation of Lymphocytes in Immune Response and Tumor Cells

Wei-ping Zeng[1,*], Shuangshuang Yang[2] and Baohua Zhou[2]

[1]Therazwimm Corporation, 3128 Ferguson Road, Huntington, WV 25705

[2] Wells Center for Pediatric Research, Department of Pediatrics, Indiana University School of Medicine, Indianapolis, IN 46202

[*]Correspondence: Wei-ping Zeng, Therazwimm Corporation, 3128 Ferguson Road, WV 25705, USA. E-mail: weipingzengny@gmail.com. Orcid iD: 0000-0002-8268-3583

Abstract

Cancer and highly proliferating normal cells have high demand for energy but paradoxically switch energy production from the highly efficient mitochondrial respiration to the low efficient cytosolic glycolysis. This phenomenon is known as the Warburg effect, but the reason for which is not fully understood. This study found that low intracellular pH (pHi) induced apoptosis, whereas high pHi enhanced proliferation, of normal lymphocytes. In tumor cells, low pHi also induced apoptosis whereas high pHi maintained high rates of proliferation. In the draining mediastinal lymph nodes (MLNs) of mice sensitized and challenged with ovalbumin, lymphocytes had dramatically higher and more heterogeneous pHi values than lymphocytes in the non-draining lymph nodes. The pHi values of the lymphocytes were inversely related to mitochondrial energetic activities, and the rise of the lymphocyte pHi in the MLNs was accompanied by the reduction of mitochondrial energetic activities. Furthermore, high lymphocyte proliferation in the MLNs powered by strong mitochondrial energy led to low pHi thereby predestined the lymphocytes to death by apoptosis, thus prevented such cells from accumulating in the MLNs. Since unlike mitochondrial respiration, the Warburg effect does not increase protons in the cells, these findings support a proposed explanation for the Warburg effect as a substitution for mitochondrial respiration that allows the highly proliferating cells to avoid low pHi-induced apoptosis.

Introduction

Cell death and proliferation play fundamental roles in numerous biological processes throughout the life cycle of an organism. In humans and animals, cell death and proliferation are key to understanding immune response and tumorigenesis. An immune response commences with lymphocyte clonal expansion and ends with the death of most of the expanded lymphocytes by apoptosis, in which mitochondria play critical roles (reviewed in (Hildeman et al., 2002; Kalkavan and Green, 2018)). Unlike normal lymphocytes, tumor cells are characteristically resistant to death, and can endlessly proliferate. In many tumor cells, the genes for apoptosis inhibitors are over expressed or amplified whereas genes for apoptosis activators are suppressed or deleted (Czabotar et al., 2014). On the other hand, mammalian cell proliferation is primarily controlled at the "restriction point" by retinoblastoma family proteins (pRB) (Friend et al., 1986; Weinberg, 1995). Mitogenic stimulation leads to the phosphorylation of the pRB proteins (Akiyama et al., 1992; Ewen et al., 1993; Hinds et al., 1992; Kato et al., 1993). Phosphorylated pRB proteins dissociate from E2F family transcription factors to allow the latter to activate target gene expression, which drives the cell to pass the restriction point, transition from G1 to S phase, and commit to completing the cell cycle (Chellappan et al., 1991; Dyson et al., 1993). These events take place from the cell membrane to the cytosol and nucleus, but largely outside the mitochondria.

However, mitochondria are efficient energy producers through aerobic respiration. Given the increased demand for energy by the proliferating cells, one might expect that mitochondria positively regulate both apoptosis and proliferation. On the contrary, almost a century ago Otto Warburg proposed that cell malignant transformation includes a precancerous phase, in which the cell must incur irreversible "injury of respiration" or "uncoupling of respiration and

phosphorylation". In fact, Warburg observed that tumor cells switch energy production from mitochondrial respiration to glycolysis, which is followed by pyruvate fermentation and excretion of the fermentation waste product lactic acid (Warburg, 1923; Warburg, 1956). This phenomenon has come to be known as the "Warburg effect", and later found in 70-80% human cancers, and shared by both tumor and normal proliferating cells including lymphocytes (Duvel et al., 2010; Vaupel and Multhoff, 2021; Wang et al., 1976). More recently, studies have identified the PI3K/AKT/mTOR pathway as the mechanism for promoting the Warburg effect. This pathway directly or through HIF-1α regulates glucose import to the cell and the expression or activities of metabolic enzymes that favor glycolysis over mitochondrial carbon oxidation (Saxton and Sabatini, 2017; Vander Heiden et al., 2009; Waickman and Powell, 2012). Studies have also unveiled an unexpected role of energy metabolism in T cell subset differentiation. It is found that T helper effector cells preferentially use glycolysis whereas Treg cells and memory CD8 T cells preferentially use mitochondrial respiration to produce energy (Araki et al., 2009; Delgoffe et al., 2009; Lee et al., 2010; Michalek et al., 2011; Pearce et al., 2009; Shi et al., 2011; Wang et al., 2011; Xu et al., 2021).

Many studies have also investigated the biological consequences of the extracellular acidosis caused by the Warburg effect. The acidic tumor microenvironment promotes tumorigenesis by facilitating tumor cell invasion of local tissues (Corbet and Feron, 2017; Estrella et al., 2013). Overactive acid extrusion and sequestration in organelles such as the Golgi apparatus lead to higher intracellular pH (pHi) in tumor cells than untransformed cells (Galenkamp and Commisso, 2021; Stock and Pedersen, 2017). The elevated pH is required for the optimal activities of a number of enzymes in the glycolytic and pentose phosphate pathways (Alfarouk et al., 2020; Galenkamp and Commisso, 2021), which appears to form a positive

feedback loop between the Warburg effect and high pHi to promote tumorigenesis. However, the contribution of the other aspect of the Warburg effect the reduction or loss of mitochondrial respiration to the high pHi in the tumor cells is unknown.

The extracellular acidosis is also a long recognized feature of inflammation (Dubos, 1955). In general, extracellular acidosis dampens the effector functions and anti-tumor activities of innate immune cells such as the neutrophils, tumor-associated macrophages and NK cells (Behnen et al., 2017; Colegio et al., 2014; Fischer et al., 2000; Gabig et al., 1979). It also suppresses T cell-mediated immunity by inhibiting cytotoxicity and blocking cell cycle progression and the expression of IL-2 and IFN-γ (Bosticardo et al., 2001). Unlike in the tumor cells, alkaline pHi resulted from overactive acid extrusion has not been reported in immune cells. To the contrary, experimentally induced extracellular acidosis lowers the pHi of T cells, which inhibits lactic acid excretion and glycolysis (Fischer et al., 2007; Wu et al., 2020).

However, the salient feature of the Warburg effect is its low efficiency of energy production as it produces only 2 ATPs per glucose whereas glycolysis followed by mitochondrial respiration produces up to 34 ATPs (Mookerjee et al., 2017). Despite the extensive studies of the mechanisms for promoting the Warburg effect and its biological consequences, why proliferating cells adopt such low-efficiency energy metabolism remains poorly understood. It cannot be explained by mitochondrial injury as originally suggested by Warburg because mitochondria in most tumor cells and normal proliferating cells are not “injured” but functional (Potter et al., 2016; Vaupel and Multhoff, 2021). Thus, it is even more baffling why the low energy efficient Warburg effect occurs even under normoxic and nutrient poor conditions (Wu et al., 2013). Given the high demand for energy, it would seem more logical for the proliferating cells to use mitochondrial respiration instead of the Warburg effect to produce ATPs from

limited fuel. One theory to explain this paradox is that the Warburg effect can produce ATPs at faster speed (Epstein et al., 2017; Pfeiffer et al., 2001). Another theory is that the Warburg effect increases glycolysis intermediate products, which are diverted to biomass synthesis (Vander Heiden et al., 2009). However, contradicting evidence and alternative explanations of the experimental data challenge these theories (Liberti and Locasale, 2016). In any case, the Warburg effect under these theories is considered to play auxiliary but not indispensable roles in cell proliferation.

In contrast, this article shows that low pHi induces apoptosis whereas high pHi allows a cell to proliferate at high rate. Furthermore, strong mitochondrial energetic activity is linked to low pHi. High proliferation powered by the strong mitochondrial energetic activity predestines the cells to death by apoptosis. Therefore, mitochondria do in fact control both cell death and proliferation by regulating pHi, and the Warburg effect may be viewed as an indispensable means for the highly proliferating cells to avoid excessive mitochondrial respiration hence low pHi-induced death.

Results

Enrichment of highly proliferating lymphocytes in pHi-high cell populations

The current study originated from an observation that an acidic solution used to prepare a test composition caused thymic atrophy. Since thymus is one of few organs in adult mice that maintain dynamic cell proliferation and death, this observation suggested a role of pH in the regulation of these two processes. To determine whether there is a natural relation between pHi and proliferation, lymph node (LN) cells were labeled with CFSE, and cultured with either IL-2 or anti-CD3 antibodies plus IL-2 for the study of T cell proliferation, or alternatively with either IL-4 or the B cell mitogen lipopolysaccharide (LPS) plus IL-4 for the study of B cell

proliferation. Lymphocyte proliferation was measured by the serial dilution of the CFSE signals after each cell division, whereas pHi was measured by the fluorescence intensity of the pH indicator pHrodo™ Red that inversely correlates with pHi. Proliferating lymphocytes were detected even in cultures with IL-2 or IL-4 alone, indicating the pre-existence of proliferating cells prior to anti-CD3 or LPS stimulation. (Fig. 1a, b). As expected, proliferating cells ($CFSE^{lo}$) increased with concurrent decrease of non-proliferating cells ($CFSE^{hi}$) after stimulation by anti-CD3 antibodies or LPS. Even the pre-existent proliferating cells underwent further divisions as evidenced by the decrease of their CFSE signals. (Fig. 1a and b). Importantly, the highly proliferating cells that had undergone more than 3 divisions were primarily found in the cell populations with high pHi, whereas cells that had fewer than 3 divisions were in cell populations with low pHi. (Fig. 1a and b).

Modulation of proliferating lymphocyte populations by pH modifiers in vitro

Further experiments were conducted to determine whether pHi is functionally relevant to lymphocyte proliferation. To this end, we first determined whether pHi could be altered by treating the lymphocytes with a low concentration of pH modifiers. Ex vivo primary lymphocytes were incubated in FBS supplemented with 10% saline or saline plus 87.5mM HOAc or NaOH in a 37°C water bath. Such in vitro culture system was designed to be free of interference by pH buffering agents in common tissue cultures. After the incubation, HOAc treatment lowered whereas NaOH treatment raised the pHi of total lymphocytes, CD4, CD8 T cells and B cells. (Fig. 2a upper). Like the in vitro treatments, in vivo treatments by injecting mice with saline plus the pH modifiers also altered the pHi of the peripheral lymphocytes of the mice. (Fig. 2a, lower). The in vitro treatments also altered the pHi of the T and B cell tumor cell lines Jurkat and Raji, respectively. (Fig. 2b).

Having demonstrated that treatment with simple acid or base is an effective way to alter pHi, we investigated the effects of the in vitro treatments on lymphocyte proliferation by analyzing the expression of Ki-67 in the lymphocytes. Ki-67 is a widely used, dependable marker for proliferating cells whose level of expression positively correlates with rRNA and DNA synthesis (Darzynkiewicz et al., 2015). In primary LN cells, the in vitro treatments with HOAc or HCl eliminated almost all Ki-67$^+$ cells. In contrast, treatment with NaOH caused about 3-fold increases of the percentages of Ki-67$^+$ cells in the total lymphocytes, CD4 and CD8 T cells, and B cells as compared with saline treatment. (Fig. 3a, d). The same analyses were also performed with LN cells derived from in vitro cultures stimulated with anti-CD3 antibodies plus IL-2 or LPS plus IL-4 but with half of the concentration of the pH modifiers because the in vitro cultured cells were less tolerant to the treatments. Similar negative and positive effects of acidic and alkaline treatments, respectively, on the lymphocyte proliferation were observed but to lesser degrees likely because of the lower concentration of the pH modifiers. (Fig. 3b, c and d). The only exception was the CD8 T cells of the LPS-stimulated cultures, in which the acid treatments did not decrease the percentages of the Ki-67$^+$ cells. (Fig. 3c, d). However, it is worth noting that in such CD8 T cells only low levels of Ki-67 were expressed, indicating that cells of low proliferative statuses were less susceptible to the acid treatments. (Fig. 3c).

Alteration of lymphocyte populations by pH modifiers in vivo

Ovalbumin (OVA)-sensitized mice were intratracheally (i.t.) challenged with OVA, and subject to in vivo treatments with saline or saline plus HOAc, HCl or NaOH. The DLN, i.e., the mediastinal lymph nodes (MLNs), were harvested 7 days after the first (or 3 days after the last) of three challenges and treatments. (Fig. 4a, upper). The total numbers of MLN cells in the HOAc-treated mice were greatly reduced as compared with those in the control saline-treated

mice. The numbers of total MLN cells in the HCl-treated mice were also significantly reduced but to lesser degrees. In contrast, treatment with NaOH mildly increased the total numbers of MLN cells. (Fig. 4a, lower). The differences in the total MLN cells were not due to differences in Treg cells because Treg cell populations in the MLNs were similar among the different treatment groups (manuscript in preparation).

The total MLN lymphocytes consisted of populations of relatively small sizes and low granularities (Lym1) and populations of larger sizes and higher granularities (Lym2). The combined percentages of Lym1 and Lym2 in the total MLN cells were similar in all treatment groups. However, while the relative proportions of Lym1 and Lym2 were similar among the saline, HCl and NaOH treatment groups, the relative proportion of Lym 2 increased in the HOAc-treated mice. (Fig. 4b, upper). Lym2 consisted mostly of B lymphoblasts, (Fig. 4b, lower right), thus indicating that B cells were less susceptible than T cells to the depletion by HOAc. Indeed, the percentages of both CD4 and CD8 T cells in Lym2 were greatly reduced in the HOAc-treated mice, whereas they were similar among the saline, HCl, and NaOH treatment groups. (Fig. 4b, lower right).

Within the Lym1, the percentages of CD4 and CD8 T cells in the HOAc-treated mice were reduced, but the percentage of B cells was higher due to the decrease of the T cells, again showing that B cells were less susceptible to the depletion by HOAc. (Fig. 4b, lower left). The percentages of CD4, CD8 T cells and B cells in the Lym1 of the HCl-treated mice were similar to those of the saline-treated mice. In the NaOH-treated mice, the percentages of CD4 and CD8 T cells were slightly decreased, whereas that of B cells was accordingly increased. (Fig. 4b, lower left). Similar depletion of the lymphocytes by the acids were also observed in MLNs

harvested at an earlier time of 3 days after the first of two OVA challenges and 1 day after only one acid treatment (from hereon referred to as the earlier time point). (Fig. S1a, b).

Positive correlation between lymphocyte proliferative status and susceptibility to depletion by acids in vivo

The Lym1 populations had very few Ki-67^{hi} cells, but about 70% of the cells expressed low levels of Ki-67 in all treatment groups. (Fig. 4c). However, in the MLNs harvested at the earlier time point, the percentage of Ki-67^{lo} Lym 1 cells in the HOAc treatment group was less than half of that in the saline-treated mice, demonstrating that even the Ki-67^{lo} cells could be depleted by the HOAc treatment in vivo. (Fig. S1c). At the later time point, the percentage of Ki-67^{hi} Lym1 B cells was lower in the HOAc-treated mice than in the saline-treated mice; and smaller reduction was also observed in the HCl-treated mice. (Fig. 4c). Similar results were observed in the MLN cells harvested at the earlier time point. (Fig. S1c).

The Lym2 populations were much more proliferative than the Lym1 populations. HOAc treatments decreased the percentages of Ki-67^{hi} Lym2 and Lym2 B cells. (Fig. 4c). Although the percentages of Ki-67^{hi} Lym2 and Lym2 B cells in the HCl–treated mice were similar to those of the saline-treated mice (Fig. 4c), their Ki-67 levels were much lower than their counterparts in the saline-treated mice, demonstrating an inhibitory role of HCl treatments in proliferation (Fig. S2). At the earlier time point, reductions of the percentages of Ki-67^{hi} cells of Lym2 and Lym2 B cells were observed in both the HOAc- and HCl-treated mice with more reduction in the HOAc-treated mice. (Fig. S1c). (Fig. 4c). In contrast, the percentages of Ki-67^{lo} cells in the acid-treated mice were either similar to or higher (due to lower percentages of Ki-67^{hi} cells) than in the saline-treated mice. (Fig. 4c).

In summary, the in vivo acid treatments generally showed lesser effects than the in vitro treatments on depleting proliferating lymphocytes because lymphocytes of high proliferative statuses (Ki-67^{hi}) are more susceptible to depletion by the acids than lymphocytes of low proliferative statues (Ki-67^{lo}) whereas in vitro acid treatments almost completely depleted both populations. The in vivo studies also revealed that T cells were more susceptible than B cells to the depletion.

The differences between the in vivo and in vitro treatments could be attributable to the complexity and fluidity of the in vivo environment. For example, the transportations of the pH modifiers into and out of the MLNs were dynamic processes. The actual concentrations of the pH modifiers at which the pH modifiers acted on the lymphocytes in the MLNs could be lower, and the durations of their actions shorter, than in the in vitro treatments. In addition, circulating or newly activated lymphocytes could replenish the MLNs after each acid treatment, therefore masking the full effects of the treatments.

Increase of the percentages of highly proliferating lymphocytes by alkaline treatments in vivo

The percentages of Ki-67^{hi} lymphocytes in NaOH-treated and saline-treated mice were compared. Higher percentages of Ki-67^{hi} Lym1 cells, Lym2 cells and Lym2 B cells were detected in NaOH-treated mice, whereas the percentages of Ki-67^{hi} Lym1 B cells were similar. (Fig. 4c). Again, the increases of Ki-67^{hi} cells by the in vivo NaOH treatments were less robust than those in the in vitro treatments, possibly for the aforementioned reasons.

Induction of apoptosis of lymphocytes by low pH

Having analyzed the effects of pH modifiers on lymphocyte proliferation, studies were carried out to investigate the role of pH in the death of lymphocytes. In vitro staining of steady-state peripheral lymphocytes of unimmunized mice with Annexin V and 7AAD showed about

5% apoptotic cells in total lymphocytes and a similar percentage of early apoptotic live cells (Annexin V^{hi} 7-AAD^{-}) (see (Vermes et al., 1995; Winklmayr et al., 2019) for the definition of early apoptotic cells); and the apoptotic and early apoptotic cells were found in CD4, CD8 T cells and B cells. (Fig. 5a). Since direct measurement of pHi of apoptotic (dead) cells was not possible due to their leaky cell membranes, early apoptotic live cells were analyzed as proxies of apoptosis. In all live lymphocyte populations, the early apoptotic cells were detected primarily in cells of low pHi. (Fig. 5b). Apoptotic and early apoptotic cells were also detected in the MLNs of mice sensitized and challenged with OVA. (Fig. 5c). Similarly to the steady-state lymphocytes, cells of low pHi in the MLNs were enriched with early apoptotic cells (Annexin V^{hi} live cells). (Fig. 5d). Although early apoptotic cells were also detected in cells of relatively high pH (in quadrant 1 of Fig. 5d), these early apoptotic cells had lower pHi than their non-apoptotic counterparts (in quadrant 4). (Fig. S3).

The detection of early apoptotic cells mainly in the pHi^{lo} cells and the depletion of lymphocytes by acid treatments in Figs. 3 and4 suggested that acid treatment induced cell death by apoptosis. To confirm this notion, MLN cells were treated in vitro by pH modifiers. After in vitro treatments with HOAc, more than 70% of the MLN cells were apoptotic whereas only 1.35% and 2.43% of the cells were apoptotic cells after saline or NaOH treatment, respectively. (Fig. 5e, far left panels). Nonetheless, regardless of the treatments, early apoptotic cells were again found primarily in the pHi^{lo} populations. (Fig. 5f). Similar results were obtained with lymphocytes derived from in vitro cultures. (Fig. S4b, d). These results showed that low pHi was a causal factor in the apoptosis of the lymphocytes.

Interconnections among mitochondrial energetic activities, pHi, apoptosis and proliferation

Since proliferating cells have high demand for energy, the findings that early apoptotic cells have low pHi and highly proliferating cells were most susceptible to acid-induced death further suggested a role of energy metabolism in apoptosis. Energy production through mitochondrial respiration could cause net accumulation of protons due to CO_2 production and electron and proton leaks (Rolfe and Brown, 1997; Tripp et al., 2001). To experimentally investigate this possibility, mitochondrial energetic activity was assessed by mitochondrial membrane potentials (MMP) in ex vivo lymphocytes from mice sensitized and challenged with OVA. In the non-draining lymph nodes (NDLNs), the majority of the lymphocytes had high MMP and low pHi. In the MLNs, the pHi of the lymphocytes dramatically increased while their MMP decreased. As a result the MLN lymphocytes became much more heterogeneous in their pHi and MMP. (Fig. 6a).

Despite the reduction, most lymphocytes in the MLNs still had substantial MMP, which was consistent with the finding that recall immune response is preferentially powered by mitochondrial energy. (Araki et al., 2009; Pearce et al., 2009). However, the B cells, CD4 and CD8 T cells in the MLN were heterogeneous with regard to their MMP and pHi. (Fig. 6b left). To further investigate the relation between MMP and pHi, the majority of these lymphocytes were divided into R1 to R4 populations based on MMP and pHi profiles. Cells of high MMP were found to have the low pHi in all types of lymphocytes (R1 and R2), whereas cells of medium or low MMP have high pHi (R3 and R4). (Fig. 6b left). Scatter plots of pHi as the function of MMP showed a negative correlation between MMP and pHi. (Fig. 6b middle). It was noteworthy that the R1 and R2 cells were of low percentages. Given that low pHi led to lymphocyte apoptosis as shown in Fig. 5 and Fig. S4, the low percentages of the R1 and R2 cells suggested that they might be constantly undergoing apoptosis therefore could not accumulate in

the MLNs. Indeed, comparisons among the cells of R1 to R4 showed that early apoptotic (Annexin V^{hi}) cells were found only in the R1 and R2 populations. (Fig. 6b left). Despite their low percentages, the R1 and R2 cells, particularly the R1 cells, contained cells of the highest rates of proliferation as judged by the levels of Ki-67 expression. (Fig. 6c). Therefore, high proliferation powered by strong mitochondrial energy production led to low pHi and predestined the cells to death by apoptosis, which prevented the cells from accumulating in the MLNs.

However, in T cells, particularly CD4 T cells, quite a few cells with low MMP also had low pHi (the Rei populations) (Fig. S5a). The low pHi in cells could not be attributed to high MMP, rather it was likely the result of imbalance between ATP hydrolysis and synthesis due to insufficient mitochondrial ATP output. Nonetheless, consistent with their low pHi, most of the Rei cells were also Annexin V^{hi} early apoptotic cells. (Fig. S5b).

Modulation of tumor cell viability and proliferation with pH modifiers

Cell proliferation is a common feature of immune response and tumorigenesis. The fact that pH modifiers could alter pHi of Jurkat and Raji cells, (Fig. 2b), suggested that proliferation and apoptosis in tumor cells could also be controlled with the pH modifiers. Indeed, HOAc treatment greatly reduced the viabilities of the Jurkat and Raji cells as determined by Trypan Blue staining, whereas NaOH treatment only slightly decreased the viabilities. (Fig. 7a). The effects of HCl treatments on the tumor cell viability were similar to those of the HOAc treatments. (Fig. S6). After saline treatment, the majority of live Jurkat cells remained Ki-67^{+}. However, few, if any, (<2%) live Jurkat cells were Ki-67^{+} after the HOAc treatment. In Raji cells, HOAc treatment dramatically reduced the percentage of Ki-67^{hi} cells as compared with saline treatment. (Fig. 7b). Therefore, like in the lymphocytes the susceptibilities of the tumor cells to acid-induced death positively correlated with their proliferative statuses. Unlike the

HOAc treatments, the percentages of Ki-67^{+} Jurkat cells and Ki-67^{hi} Raji cells after NaOH treatments were similar to those after saline treatments. (Fig. 7b).

Induction of tumor cell apoptosis by low pH

Apoptotic Jurkat and Raji cells were detected in all treatment groups. (Fig. 7c, d upper panels). The percentages of apoptotic cells detected in the saline and NaOH treatment groups were much higher than the percentages of dead cells determined by Trypan Blue staining in Fig. 7a. This discrepancy was due to additional apoptotic cell death caused by the removal of the tumor cells from the FBS and incubation in serum free buffers at 37°C and room temperature during the staining with the pH indicator and Annexin V. Conversely, many cells that had died earlier in the HOAc treatment groups had disintegrated during the staining processes. Nonetheless, regardless of the treatments, early apoptotic cells were enriched in cells of low pHi. (Fig. 7c, d lower panels). Although early apoptotic cells were also found in some pH^{hi} Jurkat cells, these pH "high" early apoptotic cells had stronger staining of the pH indicator hence lower pHi than their non-apoptotic pH^{hi} counterparts. (Fig. 7c lower panels). Thus like in the lymphocytes, low pHi triggered apoptosis of the tumor cells.

Discussion

While previous studies of the biological consequences of the Warburg effect as related to pH regulation focused on extracellular acidosis and overactive acid extrusion, the present study focuses on pHi and the reduction of mitochondrial respiration in normal lymphocytes and tumor cells. It was found that highly proliferating cells accumulated in cell populations of high pHi, whereas early apoptotic cells had low pHi. Treatments of the cells with small amounts of acid and base lowered and raised pHi, respectively. Consequently, the acid treatments induced apoptosis in lymphocytes and tumor cells, whereas conversely alkaline treatments enhanced and

maintained the proliferation of the lymphocytes and tumor cells, respectively. Such dichotomous effects of acid and alkaline treatments demonstrated a causal role of low and high pHi in the induction of apoptosis and the enhancement or maintenance of cell proliferation, respectively.

Consistent with the previous finding that recall immune response is preferentially supported by energy derived from mitochondrial respiration (Araki et al., 2009; Pearce et al., 2009), lymphocytes in the MLNs in response to intratracheal OVA challenges had substantial but heterogeneous MMP. The pHi of the lymphocytes in the MLNs dramatically increased as compared with that in the NDLNs. The pH rise was accompanied by reduction of MMP, whereas lymphocytes that maintained high MMP had low pHi. These two lines of reciprocal evidence support the notion that mitochondrial respiration contributes to low pHi. Considering that unlike in tumor cells increase of pHi due to overactive acid extrusion has not been reported in lymphocytes, the reduction of mitochondrial respiration could be a major, if not the only, mechanism for the rise of pHi in lymphocytes in response to antigen exposure. In contrast, both overactive acid extrusion and the reduction of mitochondrial respiration, as well as acid sequestration, may contribute to high pHi in tumor cells. Importantly, lymphocytes with the highest MMP and lowest pHi (the R1 cells) were the only cell populations that contained early apoptotic cells (Annexin V^{hi}). This result indicates that high lymphocyte proliferation powered by strong mitochondrial energy production predestined the cells to death by apoptosis.

The data in the present study show that low pHi is a natural and cell intrinsic trigger of lymphocyte apoptosis in both steady state LNs and MLNs during an active immune response. This is in stark contrast to earlier studies that used only cell lines induced by external artificial stimuli to undergo apoptosis in cultures wherefore the relevance to in vivo physiological or pathological apoptosis is unclear (Barry and Eastman, 1992; Gottlieb et al., 1996; Liu et al.,

2000; Matsuyama et al., 2000). Although cytosolic acidification was observed in these earlier studies, it was the consequence of the external artificial stimulations, and resulted from the redistribution of the contents of mitochondria injured by the external stimulations. In contrast, the low pHi observed in the present study is the result of accumulation of protons in the process of energy production by intact mitochondria. Nonetheless, this must not be construed as that mitochondrial energetic activity is the only cause of proton accumulation under natural conditions. In fact our own data show that some early apoptotic cells had low MMP (the Rei cells). The low MMP in these cells indicated insufficient energy production. Therefore, the low pHi in such cells is likely the result of imbalance between ATP hydrolysis and synthesis, which produces and removes protons from the cells, respectively.

Mitochondrial respiration (carbon oxidation and oxidative phosphorylation) can cause net accumulation of protons in the cells. For example, in the case of glucose metabolism, catabolizing 1 glucose molecule through glycolysis followed by mitochondrial carbon oxidation produces 6 CO_2, 10 ($NADH + H^+$) and 2 $FADH_2$. CO_2 can be converted to carbonic acids in the cell by carbonic anhydrase to produce protons (Meldrum and Roughton, 1933; Tripp et al., 2001). NADH and FADH2 are fed to the electron transport chain (ETC) to transfer electrons to the oxygen molecules, which in turn neutralize the protons derived from carbon oxidation to form water molecules. However electron leaks from the ETC cause incomplete stoichiometry of water formation hence the retention of portions. Likewise, there are also proton leaks from the proton gradient across the mitochondrial inner membrane created by the ETC. It is estimated that 20 to 25% of mitochondrial respiration is uncoupled from ATP synthesis. (Fantin et al., 2006; Rolfe and Brown, 1997). Therefore, in addition to CO_2, the imperfect efficiency of mitochondrial energetic processes could be another significant cause of proton accumulation in

the cells. Consequently, if mitochondrial respiration were to increase without restriction to meet the heightened energy demand of the highly proliferating cells, it would lower pHi to trigger apoptosis. This explains why highly proliferating cells must limit energy production from mitochondrial respiration and make up the lost energy production with the Warburg effect. Unlike the mitochondrial respiration, glycolysis in the Warburg effect produces no CO_2 and no net NADH + H^+ and $FADH_2$, and is pH neutral once the final product lactic acid is exported out of the cell.

Apart from the Warburg effect, glutaminolysis is another prominent feature of proliferating cells, and could be another mechanism for the proliferating cells to avoid death-triggering low pHi but still retain a level of energy production from the mitochondria. In glutaminolysis, glutamine is deaminated to produce ammonia and glutamate in the mitochondria. Glutamate is often excreted from proliferating cells (LeBoeuf et al., 2020), leaving ammonia in the cells to neutralize protons. Glutamate can also be further metabolized to pyruvate, which in turn can be metabolized to lactic acid to be excreted. Further, glutamate can be metabolized to malate. Malate and glutamate can participate in the malate-aspartate shuttle to move protons from cytosol to the mitochondrial matrix by the actions of malate dehydrogenases. Once in the matrix, the protons are ultimately "consumed" for ATP production.

The data in the present study place the pHi at the center of interrelationships connecting energy metabolism with cell proliferation and apoptosis. Such interrelationships provide a new perspective for understanding the dynamics of immune response and the survival strategy of tumor cells. At a low rate of proliferation lymphocytes may only need to use mitochondrial respiration to generate energy. As the proliferation rate increases, lymphocytes would have to increase Warburg effect to avoid the overuse of mitochondrial respiration that could lead to low

pHi and consequently apoptosis. Conceivably, as the signals for sustaining the Warburg effect and glutaminolysis subside towards the end of the immune response, highly proliferative lymphocytes would be forced to overuse mitochondrial respiration to meet their high demand for energy therefore become self-destructive. Alternatively, insufficient ATP synthesis would break the balance between ATP synthesis and hydrolysis, which would also cause death-triggering low pHi. In contrast, lymphocytes that have reached a sustainable balance between their proliferation propensities and energy production capacities would survive to become memory cells. Likewise, in tumorigenesis not only acid excretion creates an acidic extracellular microenvironment to facilitate tumor cell metastasis (Estrella et al., 2013), acid excretion and the reduction or loss of mitochondrial respiration ensure a relatively high pHi environment that allows the tumor cells to survive and proliferate at high rates.

Given these new insights into the role of pHi in energy metabolism, cell death and proliferation, strategies for manipulating cellular energy metabolism for clinical applications may need to take into consideration of pHi. In fact, in separate studies pH modifiers were used to effectively dampen inflammation in the lungs and nervous tissues and slow intestinal epithelial renewal in animal models of asthma, multiple sclerosis and obesity (manuscripts in preparation). In this regard, the present study shows that the susceptibility to low pH-induced apoptosis varies depending on the cell types and their proliferative statuses, as well as the chemical nature of the pH modifiers. Specifically, acetic acid was more effective than hydrochloric acid in inducing lymphocyte death in the MLNs; T cells were more susceptible than B cells, and the cells' proliferative statuses positively correlated with their susceptibilities. Therefore, by carefully analyzing the proliferative statues of pathological cells and normal cells and the cells' intrinsic susceptibilities and selecting the pH modifier(s), it may be possible to

achieve optimal benefits of disease treatment and prevention while minimizing adverse side effects.

Finally, it is worth noting that the Warburg effect is evolutionary conserved as similar phenomena are observed across species. For example, yeast growth accelerates as glucose concentration increases. However, when the yeast growth and glucose concentration reach critical points, the yeasts switch energy production from aerobic respiration to fermentation. This phenomenon is known as the Crabtree effect (Pfeiffer and Morley, 2014; Ziv et al., 2013). It is possible that the switch is necessary for the yeasts' survival because if aerobic respiration continues to increase to match the increase of energy demand, it could lower pHi to induce cell death. In bacteria, the Entner-Doudoroff glycolytic pathway is inefficient for energy production but counter intuitively is much more common among aerobic and facultative than anaerobic bacteria (Flamholz et al., 2013), suggesting that this pathway is needed to substitute for aerobic respiration for bacterial survival. Indeed, like the yeasts, bacteria switch to energetically inefficient metabolism when growth rate increases to a critical level (Vemuri et al., 2006). Parasites also appear to adopt similar strategy during the stages of their life cycles in mammalian hosts where nutrient supply is abundant (Homewood, 1977; Moyersoen et al., 2004; You et al., 2014). Such evolutionary conservation suggests that pH modifiers could be used to control not only immune response and tumorigenesis but also the survival and propagation of pathogens regardless of their abilities to resist current anti-microbial drugs.

Methods

Mice

Balb/c mice were purchased from Jackson Laboratory (Bar Harbor, ME) and housed in the animal facility of Charles River Accelerator and Development Lab (CRADL) (Cambridge,

MA). Animal studies were performed according to the protocols approved by the CRADL Institutional Animal Care and Use Committee.

CFSE labeling and activation of lymph node cells

Lymph node cells were washed 3 times with plain PBS. After the wash, the cells (3-5 x 10^6/ml) were incubated in 1μm Carboxyfluorescein succinimidyl ester (CFSE) (Fluka/Sigma-Aldrich, Burlington, VT) in plain PBS at room temperature for 7 minutes. After the incubation, 1/4 volume of FBS was added to stop the labeling, and cells were washed 4 times with PBS plus 1% FBS. The labeled cells were cultured with IL-2 (20 units/ml) or IL-2 plus anti-CD3 antibody (1μg/ml) (BD Pharmingen (San Diego, CA). Alternatively, the labeled cells were cultured with IL-4 (4ng/ml) or IL-4 plus lipopolysaccharide (LPS) (10μg/ml) (Sigma-Aldrich, St. Louis, MO). Two and half days later, cells were harvested for further experiments.

Measuring pHi and MMP

The pHi indicators pHrodo™ Green/Red AM were purchased from ThermoFisher Scientific (Waltham, MA), and MitoSpy Orange was purchased from Biolegend (San Francisco, CA). Cells were washed once with Live Cell Image Solution (LCIS) (Life Technoology/ThermoFisher Scientific, Grand Island, NY). Immediately prior to use, the pH indicator pHrodo™ Greenn/Red AM and the PowerLoad were mixed then diluted in the LCIS to produce working solution containing 0.5-1μM pH indicator and/or 100nM MitoSpy Orange. The cells (1-2 x 10^7/ml) were suspended in the working solution and incubated in a 37°C water bath for 30 minutes. After the incubation, the cells were washed once in LCIS containing 1% FBS. The levels of staining were analyzed by flow cytometry.

OVA sensitization, challenge and treatments of mice

OVA sensitization and challenge were performed as previously described (Rangasamy et al., 2005). Briefly, Balb/c mice were sensitized by i.p. injection of 20μg OVA (Sigma-Aldrich, St. Louis, MO) plus Alum adjuvant (Thermo Scientific, Rockford, IL). Two weeks later, the sensitization is repeated with 500μg OVA. About two weeks later, mice were challenged with 100μg OVA in 60μl saline by intratracheal (i.t.) instillation, and the challenges were repeated as described in each experiment. For treatments, mice received i.t. instillation of 60μl saline or saline containing 175mM HOAc or HCl along with OVA challenge. Since mice were less tolerant to i.t. instillation of NaOH, NaOH treatments were carried out by i.p. injection of 200μl of saline containing 87.5mM NaOH. After the challenges and treatments, mediastinal lymph nodes were collected at the times specified in the different experiments. For measuring the effect of pH modifiers on pHi of lymphocytes in vivo, unimmunized mice were i.p. injected with 200μl saline or saline plus 87.5mM HOAc or NaOH every other day for 3 times. Peripheral lymphocytes were harvested 1 day after the third injections.

In vitro treatments of lymphocytes and tumor cells

Lymph node cells (4 x 10^6 cells/ml) were incubated in FBS containing 10% of saline or saline plus 87.5mM HCl, HOAc or NaOH in 37°C water bath for 5 hours before analyses. The Jurkat and Raji cells (2 x 10^6 cells/ml) were incubated in FBS containing 10% saline or 87.5mM HCl, HOAc or NaOH prepared in saline in 37°C water bath for 3-5 hours. For measuring the alteration of pHi, cells stained for surface antigens and pHrodo^{TM} Green were treated for 20 min.

Flow cytometry

Fluorochrome-conjugated antibodies against mouse CD3, CD4, CD8, CD19 and Ki-67, and against human Ki-67, Zombie-Green/Violet fixable viability dyes and Foxp3 buffer set were purchased from Biolegend (San Diego, CA). Lymphocytes were stained for cell surface markers.

Live and dead cells were distinguished by staining the cells with Zombie dyes or 7-AAD. For Ki-67 staining, cells were fixed with CytoFix/CytoPerm buffer, washed with PBS plus 1% FBS and 1x CytoPerm buffer, and incubated with antibodies against mouse or human Ki-67. Jurkat and Raji cells were stained with Zombie-Green dye followed by fixation, permealization and staining with anti-human Ki-67. (Biolegend, San Diego, CA). For Annexin V staining, cells were washed twice with plain PBS and once with Annexin V binging buffer (10mM HEPES, pH7.4, 140mM NaCl, 2.5mM $CaCl_2$) and incubated with fluorochrome-conjugated Annexin V (Biolegend) in Annexin V binding buffer for 15min at room temperature. The cells were washed twice in Annexin V binding buffer, and re-suspended in Annexin V binding buffer. 7-AAD was added to the cells before analyzed by flow cytometry to distinguish dead and live cells.

List of supplemental materials: Fig. S1 to S6 and legends.

Author contributions: WZ conceived, designed and carried out the study, and wrote the manuscript. SY and BZ assisted with flow cytometry data acquisition.

Funding: BZ's effort was supported by the National Institute of Allergy and Infectious Diseases grant R21 AI159804 (BZ). There was no other external funding for this study.

Competing interests: WZ owns shares of Therazwimm.

References

Akiyama, T., Ohuchi, T., Sumida, S., Matsumoto, K., and Toyoshima, K. (1992). Phosphorylation of the retinoblastoma protein by cdk2. Proc Natl Acad Sci U S A *89*, 7900-7904.

Alfarouk, K.O., Ahmed, S.B.M., Elliott, R.L., Benoit, A., Alqahtani, S.S., Ibrahim, M.E., Bashir, A.H.H., Alhoufie, S.T.S., Elhassan, G.O., Wales, C.C.*, et al.* (2020). The Pentose Phosphate Pathway Dynamics in Cancer and Its Dependency on Intracellular pH. Metabolites *10*.

Araki, K., Turner, A.P., Shaffer, V.O., Gangappa, S., Keller, S.A., Bachmann, M.F., Larsen, C.P., and Ahmed, R. (2009). mTOR regulates memory CD8 T-cell differentiation. Nature *460*, 108-112.

Barry, M.A., and Eastman, A. (1992). Endonuclease activation during apoptosis: the role of cytosolic Ca2+ and pH. Biochem Biophys Res Commun *186*, 782-789.

Behnen, M., Moller, S., Brozek, A., Klinger, M., and Laskay, T. (2017). Extracellular Acidification Inhibits the ROS-Dependent Formation of Neutrophil Extracellular Traps. Front Immunol *8*, 184.

Bosticardo, M., Ariotti, S., Losana, G., Bernabei, P., Forni, G., and Novelli, F. (2001). Biased activation of human T lymphocytes due to low extracellular pH is antagonized by B7/CD28 costimulation. Eur J Immunol *31*, 2829-2838.

Chellappan, S.P., Hiebert, S., Mudryj, M., Horowitz, J.M., and Nevins, J.R. (1991). The E2F transcription factor is a cellular target for the RB protein. Cell *65*, 1053-1061.

Colegio, O.R., Chu, N.Q., Szabo, A.L., Chu, T., Rhebergen, A.M., Jairam, V., Cyrus, N., Brokowski, C.E., Eisenbarth, S.C., Phillips, G.M.*, et al.* (2014). Functional polarization of tumour-associated macrophages by tumour-derived lactic acid. Nature *513*, 559-563.

Corbet, C., and Feron, O. (2017). Tumour acidosis: from the passenger to the driver's seat. Nat Rev Cancer *17*, 577-593.

Czabotar, P.E., Lessene, G., Strasser, A., and Adams, J.M. (2014). Control of apoptosis by the BCL-2 protein family: implications for physiology and therapy. Nat Rev Mol Cell Biol *15*, 49-63.

Darzynkiewicz, Z., Zhao, H., Zhang, S., Lee, M.Y., Lee, E.Y., and Zhang, Z. (2015). Initiation and termination of DNA replication during S phase in relation to cyclins D1, E and A, p21WAF1, Cdt1 and the p12 subunit of DNA polymerase delta revealed in individual cells by cytometry. Oncotarget *6*, 11735-11750.

Delgoffe, G.M., Kole, T.P., Zheng, Y., Zarek, P.E., Matthews, K.L., Xiao, B., Worley, P.F., Kozma, S.C., and Powell, J.D. (2009). The mTOR kinase differentially regulates effector and regulatory T cell lineage commitment. Immunity *30*, 832-844.

Dubos, R.J. (1955). The micro-environment of inflammation or Metchnikoff revisited. Lancet *269*, 1-5.

Duvel, K., Yecies, J.L., Menon, S., Raman, P., Lipovsky, A.I., Souza, A.L., Triantafellow, E., Ma, Q., Gorski, R., Cleaver, S.*, et al.* (2010). Activation of a metabolic gene regulatory network downstream of mTOR complex 1. Mol Cell *39*, 171-183.

Dyson, N., Dembski, M., Fattaey, A., Ngwu, C., Ewen, M., and Helin, K. (1993). Analysis of p107-associated proteins: p107 associates with a form of E2F that differs from pRB-associated E2F-1. J Virol *67*, 7641-7647.

Epstein, T., Gatenby, R.A., and Brown, J.S. (2017). The Warburg effect as an adaptation of cancer cells to rapid fluctuations in energy demand. PLoS One *12*, e0185085.

Estrella, V., Chen, T., Lloyd, M., Wojtkowiak, J., Cornnell, H.H., Ibrahim-Hashim, A., Bailey, K., Balagurunathan, Y., Rothberg, J.M., Sloane, B.F.*, et al.* (2013). Acidity generated by the tumor microenvironment drives local invasion. Cancer Res *73*, 1524-1535.

Ewen, M.E., Sluss, H.K., Sherr, C.J., Matsushime, H., Kato, J., and Livingston, D.M. (1993). Functional interactions of the retinoblastoma protein with mammalian D-type cyclins. Cell *73*, 487-497.

Fantin, V.R., St-Pierre, J., and Leder, P. (2006). Attenuation of LDH-A expression uncovers a link between glycolysis, mitochondrial physiology, and tumor maintenance. Cancer Cell *9*, 425-434.

Fischer, B., Muller, B., Fisch, P., and Kreutz, W. (2000). An acidic microenvironment inhibits antitumoral non-major histocompatibility complex-restricted cytotoxicity: implications for cancer immunotherapy. J Immunother *23*, 196-207.

Fischer, K., Hoffmann, P., Voelkl, S., Meidenbauer, N., Ammer, J., Edinger, M., Gottfried, E., Schwarz, S., Rothe, G., Hoves, S.*, et al.* (2007). Inhibitory effect of tumor cell-derived lactic acid on human T cells. Blood *109*, 3812-3819.

Flamholz, A., Noor, E., Bar-Even, A., Liebermeister, W., and Milo, R. (2013). Glycolytic strategy as a tradeoff between energy yield and protein cost. Proc Natl Acad Sci U S A *110*, 10039-10044.

Friend, S.H., Bernards, R., Rogelj, S., Weinberg, R.A., Rapaport, J.M., Albert, D.M., and Dryja, T.P. (1986). A human DNA segment with properties of the gene that predisposes to retinoblastoma and osteosarcoma. Nature *323*, 643-646.

Gabig, T.G., Bearman, S.I., and Babior, B.M. (1979). Effects of oxygen tension and pH on the respiratory burst of human neutrophils. Blood *53*, 1133-1139.

Galenkamp, K.M.O., and Commisso, C. (2021). The Golgi as a "Proton Sink" in Cancer. Front Cell Dev Biol *9*, 664295.

Gottlieb, R.A., Nordberg, J., Skowronski, E., and Babior, B.M. (1996). Apoptosis induced in Jurkat cells by several agents is preceded by intracellular acidification. Proc Natl Acad Sci U S A *93*, 654-658.

Hildeman, D.A., Zhu, Y., Mitchell, T.C., Kappler, J., and Marrack, P. (2002). Molecular mechanisms of activated T cell death in vivo. Curr Opin Immunol *14*, 354-359.

Hinds, P.W., Mittnacht, S., Dulic, V., Arnold, A., Reed, S.I., and Weinberg, R.A. (1992). Regulation of retinoblastoma protein functions by ectopic expression of human cyclins. Cell *70*, 993-1006.

Homewood, C.A. (1977). Carbohydrate metabolism of malarial parasites. Bull World Health Organ *55*, 229-235.

Kalkavan, H., and Green, D.R. (2018). MOMP, cell suicide as a BCL-2 family business. Cell Death Differ *25*, 46-55.

Kato, J., Matsushime, H., Hiebert, S.W., Ewen, M.E., and Sherr, C.J. (1993). Direct binding of cyclin D to the retinoblastoma gene product (pRb) and pRb phosphorylation by the cyclin D-dependent kinase CDK4. Genes Dev *7*, 331-342.

LeBoeuf, S.E., Wu, W.L., Karakousi, T.R., Karadal, B., Jackson, S.R., Davidson, S.M., Wong, K.K., Koralov, S.B., Sayin, V.I., and Papagiannakopoulos, T. (2020). Activation of Oxidative Stress Response in Cancer Generates a Druggable Dependency on Exogenous Non-essential Amino Acids. Cell Metab *31*, 339-350 e334.

Lee, K., Gudapati, P., Dragovic, S., Spencer, C., Joyce, S., Killeen, N., Magnuson, M.A., and Boothby, M. (2010). Mammalian target of rapamycin protein complex 2 regulates differentiation of Th1 and Th2 cell subsets via distinct signaling pathways. Immunity *32*, 743-753.

Liberti, M.V., and Locasale, J.W. (2016). The Warburg Effect: How Does it Benefit Cancer Cells? Trends Biochem Sci *41*, 211-218.

Liu, D., Martino, G., Thangaraju, M., Sharma, M., Halwani, F., Shen, S.H., Patel, Y.C., and Srikant, C.B. (2000). Caspase-8-mediated intracellular acidification precedes mitochondrial dysfunction in somatostatin-induced apoptosis. J Biol Chem *275*, 9244-9250.

Matsuyama, S., Llopis, J., Deveraux, Q.L., Tsien, R.Y., and Reed, J.C. (2000). Changes in intramitochondrial and cytosolic pH: early events that modulate caspase activation during apoptosis. Nat Cell Biol *2*, 318-325.

Meldrum, N.U., and Roughton, F.J. (1933). Carbonic anhydrase. Its preparation and properties. J Physiol *80*, 113-142.

Michalek, R.D., Gerriets, V.A., Jacobs, S.R., Macintyre, A.N., MacIver, N.J., Mason, E.F., Sullivan, S.A., Nichols, A.G., and Rathmell, J.C. (2011). Cutting edge: distinct glycolytic and lipid oxidative metabolic programs are essential for effector and regulatory CD4+ T cell subsets. J Immunol *186*, 3299-3303.

Mookerjee, S.A., Gerencser, A.A., Nicholls, D.G., and Brand, M.D. (2017). Quantifying intracellular rates of glycolytic and oxidative ATP production and consumption using extracellular flux measurements. J Biol Chem *292*, 7189-7207.

Moyersoen, J., Choe, J., Fan, E., Hol, W.G., and Michels, P.A. (2004). Biogenesis of peroxisomes and glycosomes: trypanosomatid glycosome assembly is a promising new drug target. FEMS Microbiol Rev *28*, 603-643.

Pearce, E.L., Walsh, M.C., Cejas, P.J., Harms, G.M., Shen, H., Wang, L.S., Jones, R.G., and Choi, Y. (2009). Enhancing CD8 T-cell memory by modulating fatty acid metabolism. Nature *460*, 103-107.

Pfeiffer, T., and Morley, A. (2014). An evolutionary perspective on the Crabtree effect. Front Mol Biosci *1*, 17.

Pfeiffer, T., Schuster, S., and Bonhoeffer, S. (2001). Cooperation and competition in the evolution of ATP-producing pathways. Science *292*, 504-507.

Potter, M., Newport, E., and Morten, K.J. (2016). The Warburg effect: 80 years on. Biochem Soc Trans *44*, 1499-1505.

Rangasamy, T., Guo, J., Mitzner, W.A., Roman, J., Singh, A., Fryer, A.D., Yamamoto, M., Kensler, T.W., Tuder, R.M., Georas, S.N.*, et al.* (2005). Disruption of Nrf2 enhances susceptibility to severe airway inflammation and asthma in mice. J Exp Med *202*, 47-59.

Rolfe, D.F., and Brown, G.C. (1997). Cellular energy utilization and molecular origin of standard metabolic rate in mammals. Physiol Rev *77*, 731-758.

Saxton, R.A., and Sabatini, D.M. (2017). mTOR Signaling in Growth, Metabolism, and Disease. Cell *168*, 960-976.

Shi, L.Z., Wang, R., Huang, G., Vogel, P., Neale, G., Green, D.R., and Chi, H. (2011). HIF1alpha-dependent glycolytic pathway orchestrates a metabolic checkpoint for the differentiation of TH17 and Treg cells. J Exp Med *208*, 1367-1376.

Stock, C., and Pedersen, S.F. (2017). Roles of pH and the Na(+)/H(+) exchanger NHE1 in cancer: From cell biology and animal models to an emerging translational perspective? Semin Cancer Biol *43*, 5-16.

Tripp, B.C., Smith, K., and Ferry, J.G. (2001). Carbonic anhydrase: new insights for an ancient enzyme. J Biol Chem *276*, 48615-48618.

Vander Heiden, M.G., Cantley, L.C., and Thompson, C.B. (2009). Understanding the Warburg effect: the metabolic requirements of cell proliferation. Science *324*, 1029-1033.

Vaupel, P., and Multhoff, G. (2021). The Warburg Effect: Historical Dogma Versus Current Rationale. Adv Exp Med Biol *1269*, 169-177.

Vemuri, G.N., Altman, E., Sangurdekar, D.P., Khodursky, A.B., and Eiteman, M.A. (2006). Overflow metabolism in Escherichia coli during steady-state growth: transcriptional regulation and effect of the redox ratio. Appl Environ Microbiol *72*, 3653-3661.

Vermes, I., Haanen, C., Steffens-Nakken, H., and Reutelingsperger, C. (1995). A novel assay for apoptosis. Flow cytometric detection of phosphatidylserine expression on early apoptotic cells using fluorescein labelled Annexin V. J Immunol Methods *184*, 39-51.

Waickman, A.T., and Powell, J.D. (2012). mTOR, metabolism, and the regulation of T-cell differentiation and function. Immunol Rev *249*, 43-58.

Wang, R., Dillon, C.P., Shi, L.Z., Milasta, S., Carter, R., Finkelstein, D., McCormick, L.L., Fitzgerald, P., Chi, H., Munger, J.*, et al.* (2011). The transcription factor Myc controls metabolic reprogramming upon T lymphocyte activation. Immunity *35*, 871-882.

Wang, T., Marquardt, C., and Foker, J. (1976). Aerobic glycolysis during lymphocyte proliferation. Nature *261*, 702-705.

Warburg, O. (1923). Versuche an überlebendem Carcinomgewebe. Biochem Zschr *142*, 317–333.

Warburg, O. (1956). On the origin of cancer cells. Science *123*, 309-314.

Weinberg, R.A. (1995). The retinoblastoma protein and cell cycle control. Cell *81*, 323-330.

Winklmayr, M., Gaisberger, M., Kittl, M., Fuchs, J., Ritter, M., and Jakab, M. (2019). Dose-Dependent Cannabidiol-Induced Elevation of Intracellular Calcium and Apoptosis in Human Articular Chondrocytes. J Orthop Res *37*, 2540-2549.

Wu, C.A., Chao, Y., Shiah, S.G., and Lin, W.W. (2013). Nutrient deprivation induces the Warburg effect through ROS/AMPK-dependent activation of pyruvate dehydrogenase kinase. Biochim Biophys Acta *1833*, 1147-1156.

Wu, H., Estrella, V., Beatty, M., Abrahams, D., El-Kenawi, A., Russell, S., Ibrahim-Hashim, A., Longo, D.L., Reshetnyak, Y.K., Moshnikova, A.*, et al.* (2020). T-cells produce acidic niches in lymph nodes to suppress their own effector functions. Nat Commun *11*, 4113.

Xu, K., Yin, N., Peng, M., Stamatiades, E.G., Shyu, A., Li, P., Zhang, X., Do, M.H., Wang, Z., Capistrano, K.J.*, et al.* (2021). Glycolysis fuels phosphoinositide 3-kinase signaling to bolster T cell immunity. Science *371*, 405-410.

You, H., Stephenson, R.J., Gobert, G.N., and McManus, D.P. (2014). Revisiting glucose uptake and metabolism in schistosomes: new molecular insights for improved schistosomiasis therapies. Front Genet *5*, 176.

Ziv, N., Brandt, N.J., and Gresham, D. (2013). The use of chemostats in microbial systems biology. J Vis Exp.

Figure legends

Fig. 1. Positive correlation between lymphocyte proliferation and intracellular pH. Shown are flow cytometric pseudocolor plots and histograms of intracellular pH (inversely indicated by the fluorescence intensities of pHrodo™ Red) and/or CFSE of live lymphocytes after in vitro cultures with the indicated stimuli. Cell proliferation/division is indicated by serial reduction of the CFSE signals. Numbers in the plots are percentages of cells in each quadrant. One of three similar experiments is shown.

(a) CFSE-labeled lymph node cells stimulated in vitro with IL-2 only, or IL-2 plus anti-CD3 antibodies.

(b) CFSE-labeled lymph node cells stimulated in vitro with IL-4 only, or IL-4 plus LPS.

Fig. 2. Alteration of intracellular pH by pH modifiers. Shown are overlaid histograms of intracellular pH (inversely indicated by the fluorescence intensities of pHrodo™ Green) of live lymphocytes or tumor cells after in vitro or in vivo treatments with pH modifiers as described in the Methods. One of two similar experiments is shown. MFI: mean fluorescence intensity of pHrodo™ Green.

(a) Upper panels are primary lymphocytes in vitro treated in FBS containing 10% saline or saline plus 87.5mM HOAc or NaOH. Lower panels are ex vivo lymphocytes of unimmunized mice in vivo treated with injections of 200μl saline, or saline plus 87.5mM HOAc or NaOH.

(b) Jurkat and Raji cells in vitro treated as in (a) upper panels.

Fig. 3. Effects of in vitro treatments with pH modifiers on lymphocyte proliferation. Primary or in vitro stimulated lymph node cells were treated in FBS containing 10% saline or saline plus 87.5mM or 43.75mM HCl, HOAc or NaOH, then analyzed by flow cytometry to determine Ki-67 expression in live total lymphocytes (Lym), CD4, CD8 T cells and B cells ($CD19^+$). Numbers in the histograms are the percentages of Ki-67^+ (PE^+) cells. One of three similar experiments is shown.

(a) Primary LN cells.

(b) In vitro anti-CD3 antibody plus IL-2-stimuluated LN cells.

(c) In vitro LPS plus IL-4-stimuluated LN cells.

(d) Graphic presentation of the percentages of Ki-67^{+} (PE^{+}) cells in a, b and c.

Fig. 4. Alterations of the populations and proliferation of lymphocytes in the MLNs by in vivo treatments with pH modifiers of mice sensitized and challenged with OVA. Numbers in the flow cytometry plots are the percentages of cells. One of two similar experiments is shown.

(a) Upper: Schedules for OVA challenges and treatments of the sensitized mice. Lower: A graph showing the average total numbers of MLN cells of the mice in the different treatment groups (3 mice/group). Error bars are standard deviations. Statistical significance between the saline and the other groups was determined by Student t test; * $p < 0.05$, ** $p < 0.01$.

(b) Upper: Lym1 and Lym2 lymphocyte populations in live MLN cells. Lower: CD4, CD8 T cells and B cells (CD19^{+}) in Lym1 and Lym2.

(c) Left: Histograms of Ki-67 expression in Lym1, Lym2 and the B cells thereof. Right: Graphic presentations of the percentages of the Ki-67 high and low cells in the left panels.

Fig. 5. Low intracellular pH in early apoptotic lymphocytes and induction of apoptosis by acid treatments. Apoptotic cells (Annexin V^{hi} 7AAD^{+} or Zombie^{hi}) in total lymphocyte populations and early apoptotic cells (Annexin V^{hi}) and intracellular pH in live lymphocyte populations were detected by flow cytometry. Numbers in the plots are the percentages of cells in each quadrant.

(a and b) Steady-state peripheral lymphocytes of unimmunized mice.

(c and d) Ex vivo MLN cells of mice sensitized and challenged with OVA.

(e and f) MLN cells of the OVA-sensitized and challenged mice after in vitro treatments in FBS containing 10% saline, or saline plus 47.5mM HOAc or NaOH.

Fig. 6. Role of mitochondrial membrane potential in determining intracellular pH, apoptosis and proliferation of lymphocytes during in vivo immune response. OVA sensitized mice were challenged with OVA on day 0 and 1. Non-draining inguinal lymph nodes (NDLDs) and draining lymph nodes (MLNs) were harvested on day 3. Mitochondrial membrane potential (MitoSpy Orange), intracellular pH (pHrodo™ Green), early apoptosis and proliferation in live lymphocytes were analyzed. Numbers in the flow cytometry plots are percentages of cells. One of three similar experiments is shown.

(a) Comparisons of intracellular pH and mitochondrial membrane potentials of live total lymphocytes of NDLNs and MLNs. Left two panels are pseudocolor plots showing the mitochondrial membrane potentials and intracellular pH. Right two panels are overlaid histograms of the intracellular pH and mitochondrial membrane potentials.

(b) Left panels: the majority of live B cells, CD4, and CD8 T cells of the MLN cells were divided into R1 to R4 populations based on their pHi and mitochondrial membrane potentials. The middle panels are scatter plots showing pHi (MFI of pHrodo™ Green) as the function of mitochondrial membrane potential (MFI of MitoSpy) of the cells in R1 to R4. The right panels are overlaid histograms of Annexin V staining of the cells in R1 to R4.

(c) Cell populations similar to R1 to R4 in (b) were sorted. Shown are the overlaid histograms of the Ki-67 staining of the sorted cells.

Fig. 7. Control of the proliferation and apoptosis of tumor cells with pH modifiers. Jurkat and Raji cells were treated in FBS containing 10% of saline or saline plus 87.5mM HOAc or NaOH. Numbers in the flow cytometry plots are percentages of cells.

(a) Comparison of the average viabilities of Jurkat and Raji cells as determined by Trypan Blue staining. Error bars are standard deviations (3 replicates for each treatment). Statistical significance of differences between the saline and other treatment groups was determined by Student t test, * $p < 0.05$, ** $p < 0.01$.

(b) Histograms of Ki-67 staining in live Jurkat or Raji cells after the different treatments. One of three similar experiments is shown.

(c and d) Apoptosis of Jurkat (c) and Raji (d) tumor cells. Upper panels: 7AAD and Annexin V staining of total tumor cells after the different treatments. Lower panels: pHrodo™ Green and Annexin V staining of live ($7AAD^-$) tumor cells after the treatments. One of two similar experiments is shown.

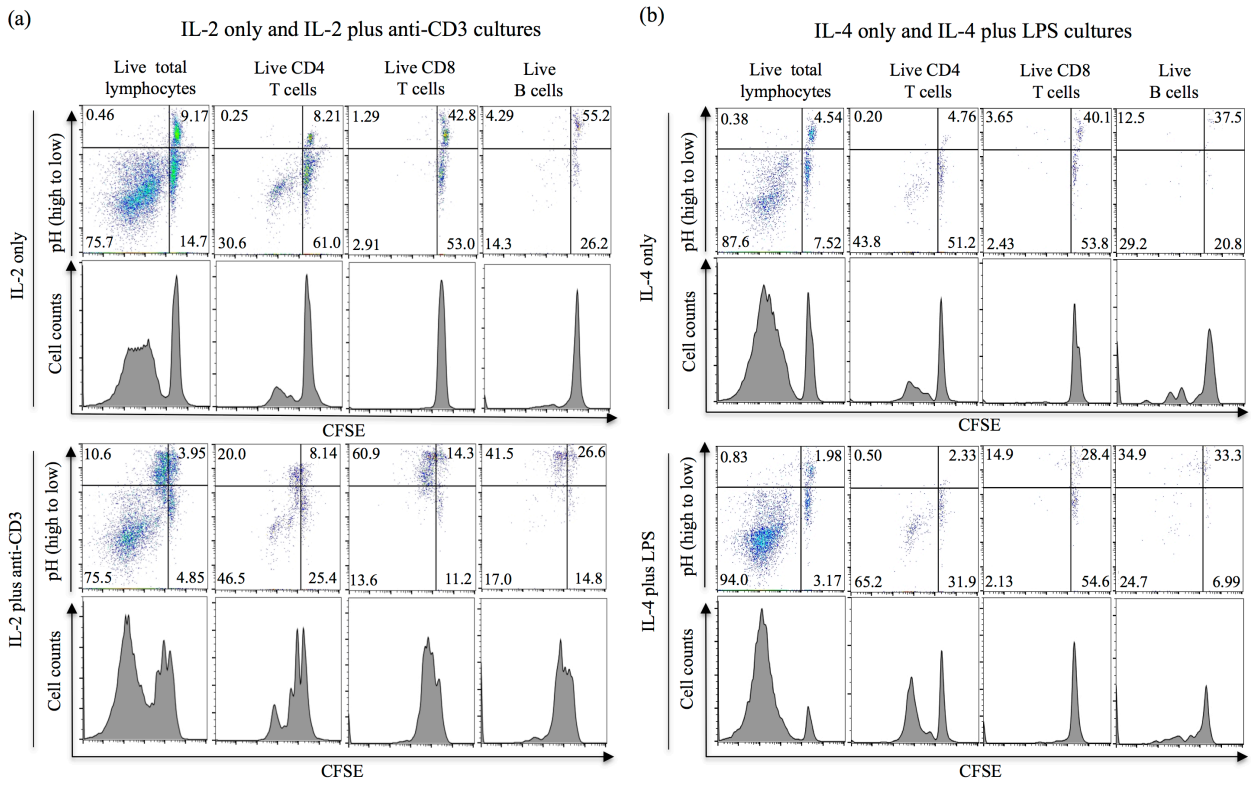

Fig. 1. Positive correlation between lymphocyte proliferation and intracellular pH. Shown are flow cytometric pseudocolor plots and histograms of intracellular pH (inversely indicated by the fluorescence intensities of pHrodo™ Red) and/or CFSE of live lymphocytes after in vitro cultures with the indicated stimuli. Cell proliferation/division is indicated by serial reduction of the CFSE signals. Numbers in the plots are percentages of cells in each quadrant. One of three similar experiments is shown.

(a) CFSE-labeled lymph node cells stimulated in vitro with IL-2 only, or IL-2 plus anti-CD3 antibodies.

(b) CFSE-labeled lymph node cells stimulated in vitro with IL-4 only, or IL-4 plus LPS.

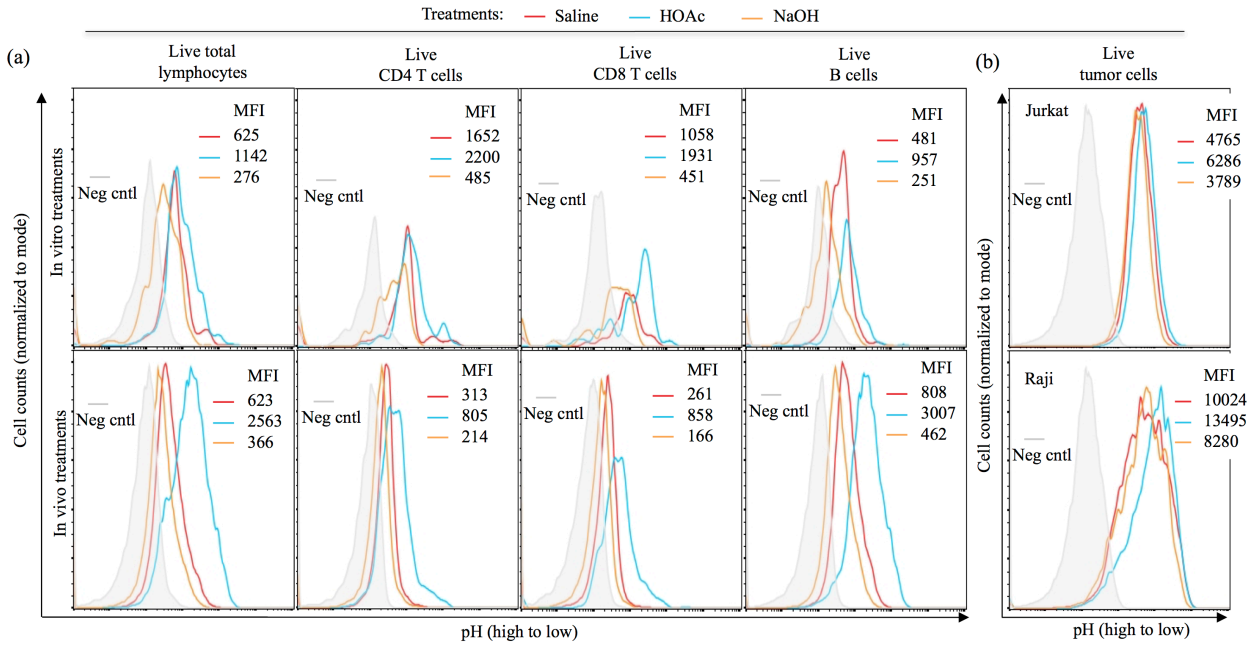

Fig. 2. Alteration of intracellular pH by pH modifiers. Shown are overlaid histograms of intracellular pH (inversely indicated by the fluorescence intensities of pHrodo™ Green) of live lymphocytes or tumor cells after in vitro or in vivo treatments with pH modifiers as described in the Methods. One of two similar experiments is shown. MFI: mean fluorescence intensity of pHrodo™ Green.

(a) Upper panels are primary lymphocytes in vitro treated in FBS containing 10% saline or saline plus 87.5mM HOAc or NaOH. Lower panels are ex vivo lymphocytes of unimmunized mice in vivo treated with injections of 200µl saline, or saline plus 87.5mM HOAc or NaOH.

(b) Jurkat and Raji cells in vitro treated as in (a) upper panels.

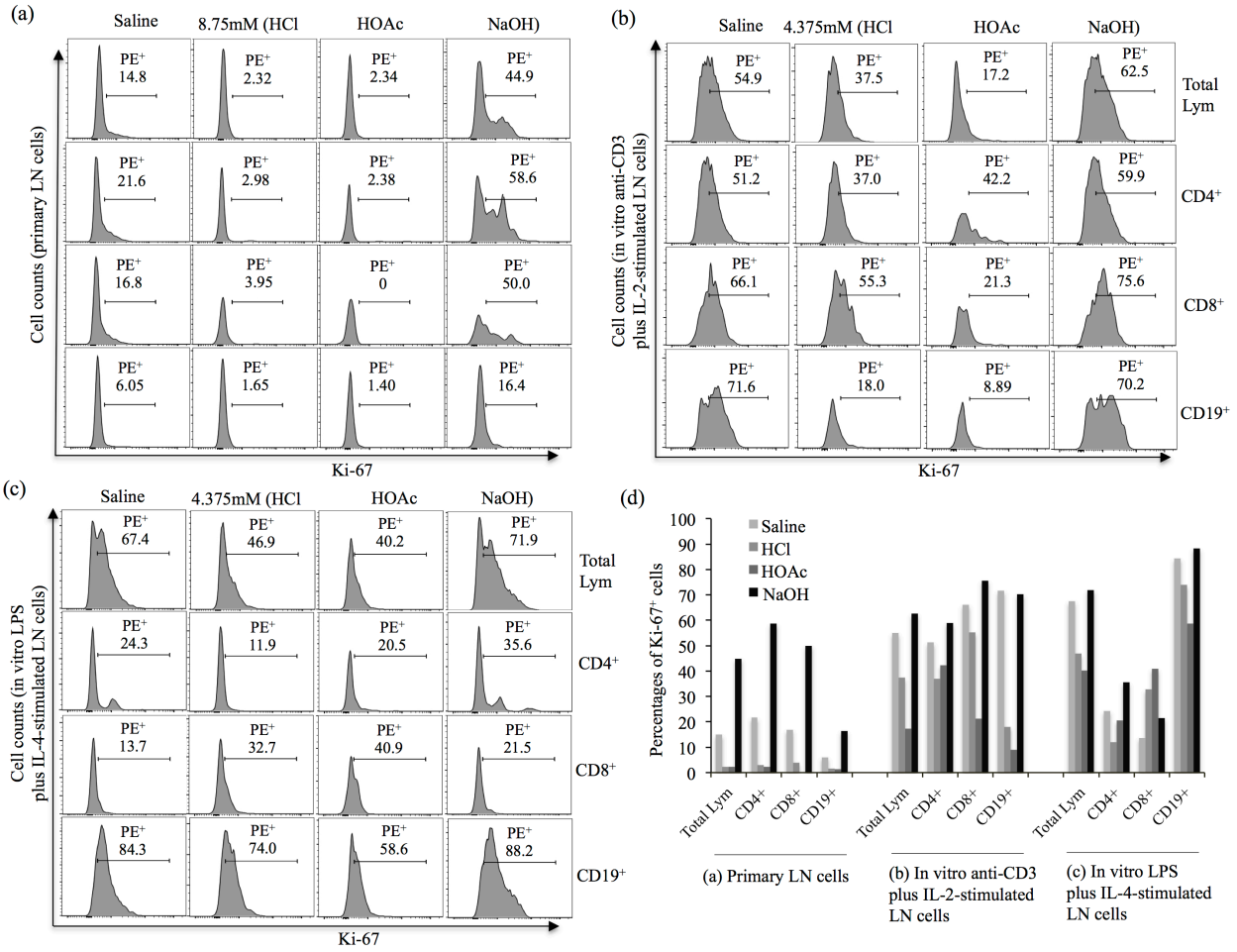

Fig. 3. Effects of in vitro treatments with pH modifiers on lymphocyte proliferation. Primary or in vitro stimulated lymph node cells were treated in FBS containing 10% saline or saline plus 87.5mM or 43.75mM HCl, HOAc or NaOH, then analyzed by flow cytometry to determine Ki-67 expression in live total lymphocytes (Lym), CD4, CD8 T cells and B cells ($CD19^+$). Numbers in the histograms are the percentages of Ki-67^+ (PE^+) cells. One of three similar experiments is shown.

(a) Primary LN cells.

(b) In vitro anti-CD3 antibody plus IL-2-stimuluated LN cells.

(c) In vitro LPS plus IL-4-stimuluated LN cells.

(d) Graphic presentation of the percentages of Ki-67^+ (PE^+) cells in a, b and c.

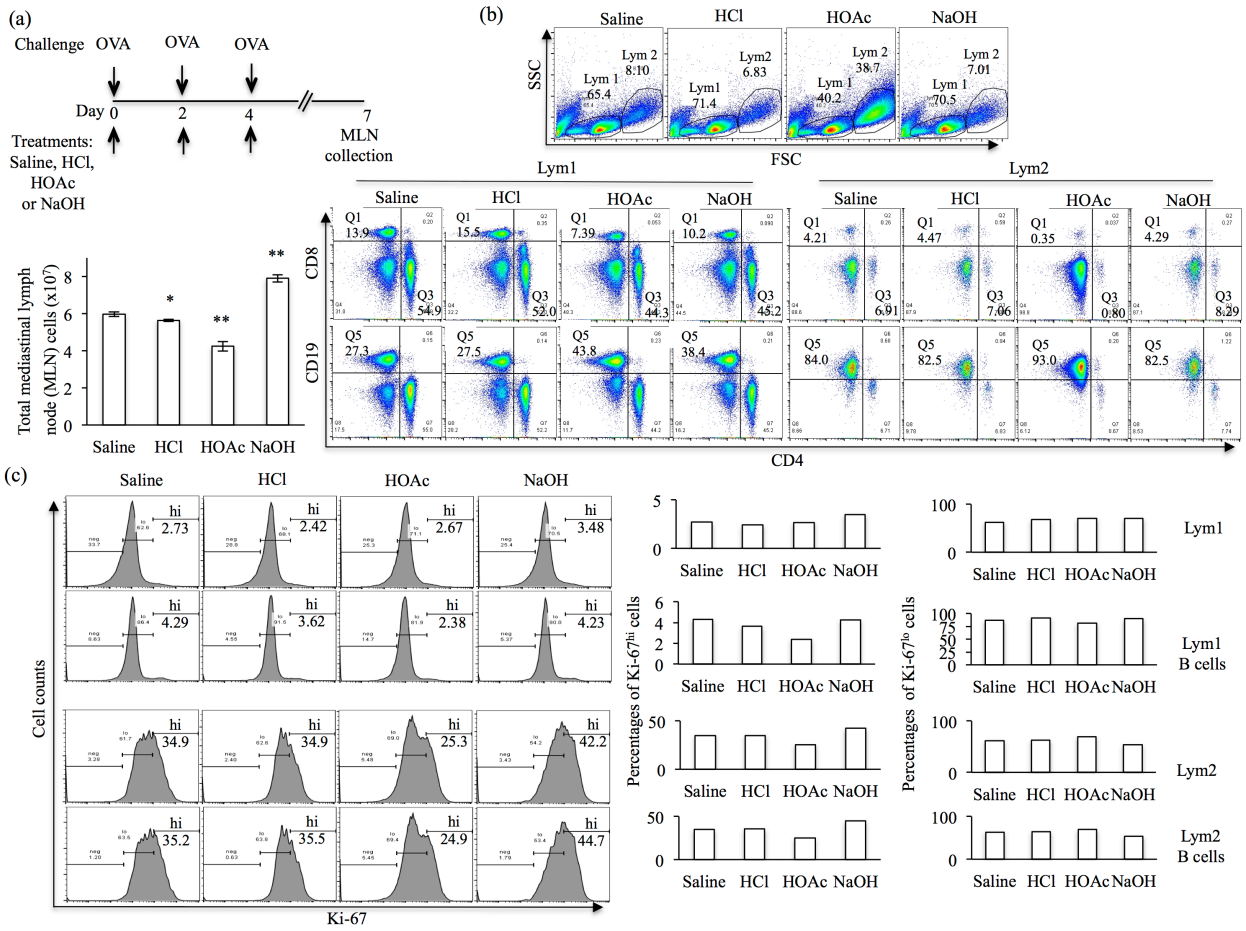

Fig. 4. Alterations of the populations and proliferation of lymphocytes in the MLNs by in vivo treatments with pH modifiers of mice sensitized and challenged with OVA. Numbers in the flow cytometry plots are the percentages of cells. One of two similar experiments is shown.

(a) Upper: Schedules for OVA challenges and treatments of the sensitized mice. Lower: A graph showing the average total numbers of MLN cells of the mice in the different treatment groups (3 mice/group). Error bars are standard deviations. Statistical significance between the saline and the other groups was determined by Student t test; * $p < 0.05$, ** $p < 0.01$.

(b) Upper: Lym1 and Lym2 lymphocyte populations in live MLN cells. Lower: CD4, CD8 T cells and B cells ($CD19^{+}$) in Lym1 and Lym2.

(c) Left: Histograms of Ki-67 expression in Lym1, Lym2 and the B cells thereof. Right: Graphic presentations of the percentages of the Ki-67 high and low cells in the left panels.

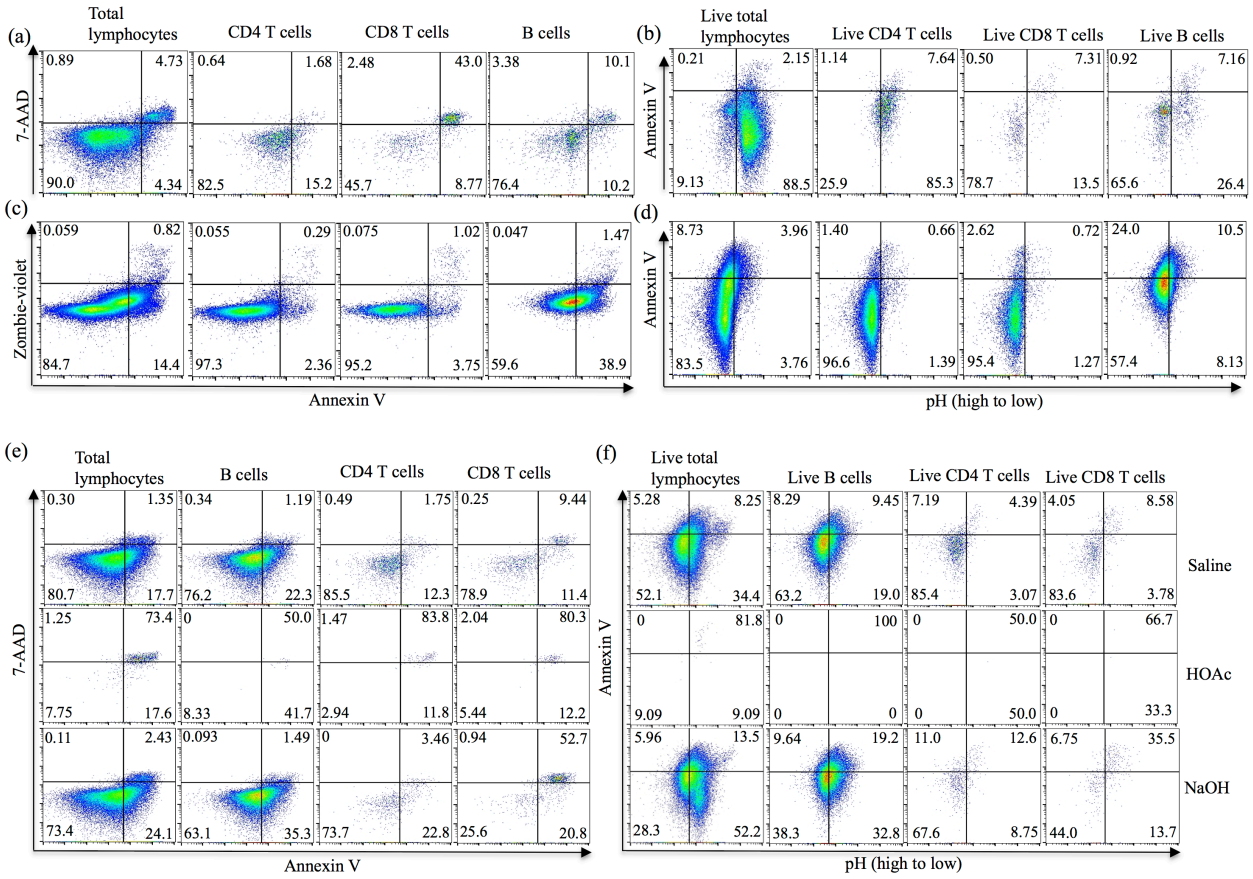

Fig. 5. Low intracellular pH in early apoptotic lymphocytes and induction of apoptosis by acid treatments. Apoptotic cells (Annexin V^{hi} $7AAD^{+}$ or $Zombie^{hi}$) in total lymphocyte populations and early apoptotic cells (Annexin V^{hi}) and intracellular pH in live lymphocyte populations were detected by flow cytometry. Numbers in the plots are the percentages of cells in each quadrant.
(a and b) Steady-state peripheral lymphocytes of unimmunized mice.
(c and d) Ex vivo MLN cells of mice sensitized and challenged with OVA.
(e and f) MLN cells of the OVA-sensitized and challenged mice after in vitro treatments in FBS containing 10% saline, or saline plus 47.5mM HOAc or NaOH.

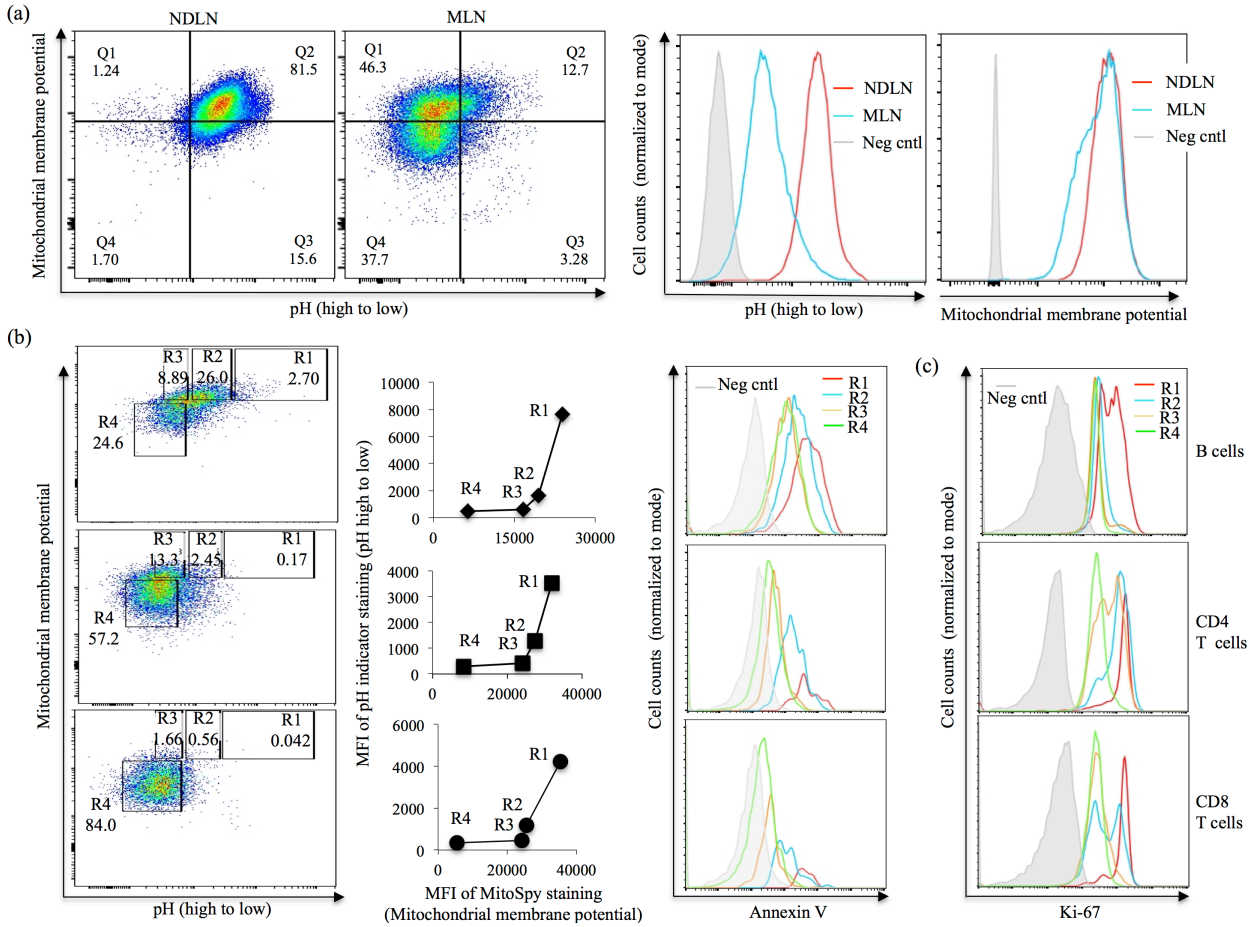

Fig. 6. Role of mitochondrial membrane potential in determining intracellular pH, apoptosis and proliferation of lymphocytes during in vivo immune response. OVA sensitized mice were challenged with OVA on day 0 and 1. Non-draining inguinal lymph nodes (NDLDs) and draining lymph nodes (MLNs) were harvested on day 3. Mitochondrial membrane potential (MitoSpy Orange), intracellular pH (pHrodo^{TM} Green), early apoptosis and proliferation in live lymphocytes were analyzed. Numbers in the flow cytometry plots are percentages of cells. One of three similar experiments is shown.

(a) Comparisons of intracellular pH and mitochondrial membrane potentials of live total lymphocytes of NDLNs and MLNs. Left two panels are pseudocolor plots showing the mitochondrial membrane potentials and intracellular pH. Right two panels are overlaid histograms of the intracellular pH and mitochondrial membrane potentials.

(b) Left panels: the majority of live B cells, CD4, and CD8 T cells of the MLN cells were divided into R1 to R4 populations based on their pHi and mitochondrial membrane potentials. The middle panels are scatter plots showing pHi (MFI of pHrodo^{TM} Green) as the function of mitochondrial membrane potential (MFI of MitoSpy) of the cells in R1 to R4. The right panels are overlaid histograms of Annexin V staining of the cells in R1 to R4.

(c) Cell populations similar to R1 to R4 in (b) were sorted. Shown are the overlaid histograms of the Ki-67 staining of the sorted cells.

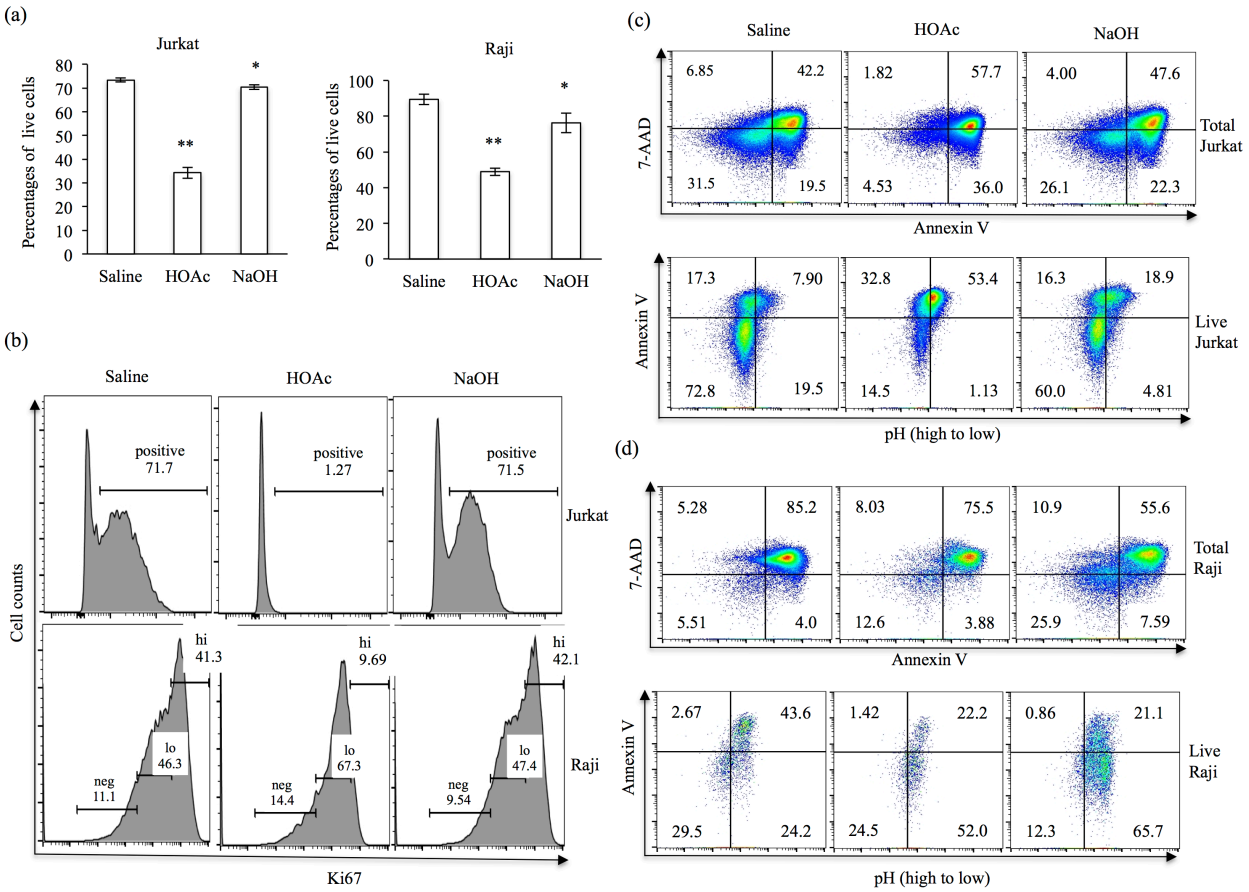

Fig. 7. Control of the proliferation and apoptosis of tumor cells with pH modifiers. Jurkat and Raji cells were treated in FBS containing 10% of saline or saline plus 87.5mM HOAc or NaOH. Numbers in the flow cytometry plots are percentages of cells.

(a) Comparison of the average viabilities of Jurkat and Raji cells as determined by Trypan Blue staining. Error bars are standard deviations (3 replicates for each treatment). Statistical significance of differences between the saline and other treatment groups was determined by Student t test, * $p < 0.05$, ** $p < 0.01$.

(b) Histograms of Ki-67 staining in live Jurkat or Raji cells after the different treatments. One of three similar experiments is shown.

(c and d) Apoptosis of Jurkat (c) and Raji (d) tumor cells. Upper panels: 7AAD and Annexin V staining of total tumor cells after the different treatments. Lower panels: pHrodo^{TM} Green and Annexin V staining of live (7AAD^{-}) tumor cells after the treatments. One of two similar experiments is shown.

Supplementary materials

Figs. S1 to S6 and legends

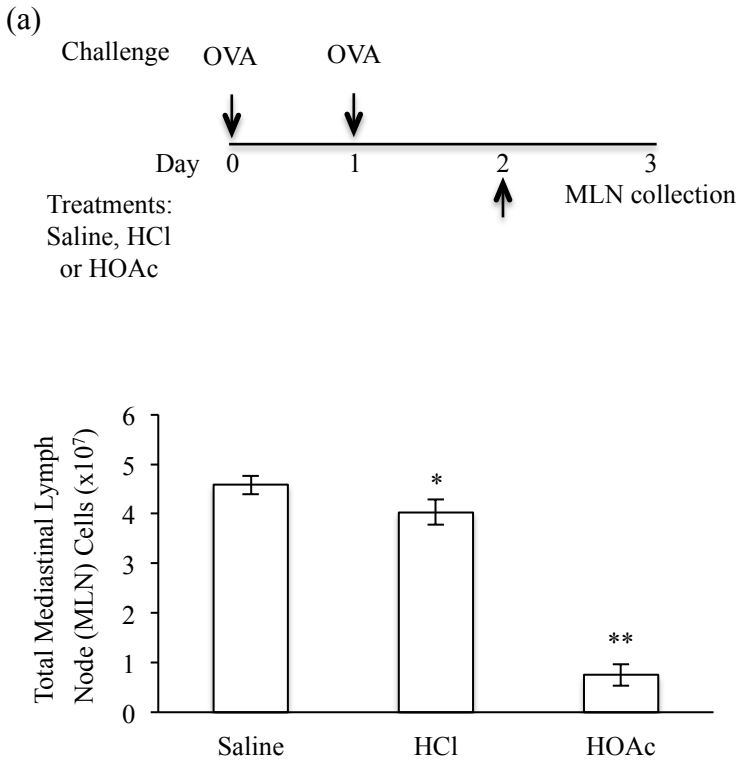

Fig. S1. Effects of pH modifiers on the populations and proliferation of lymphocytes in MLNs 3 days after initial OVA challenge.

(a) The top panel is a schematic illustrating the schedules for OVA challenges and treatments with saline, or saline plus HCl or HOAc of OVA-sensitized mice. Arrows indicate the time points of the challenges or treatments. The lower panel shows the average total numbers of MLN cells of mice in the different treatment groups. Statistical significance between saline and the other groups was determined by Student t test; * $p < 0.05$, ** $p < 0.01$.

(b)

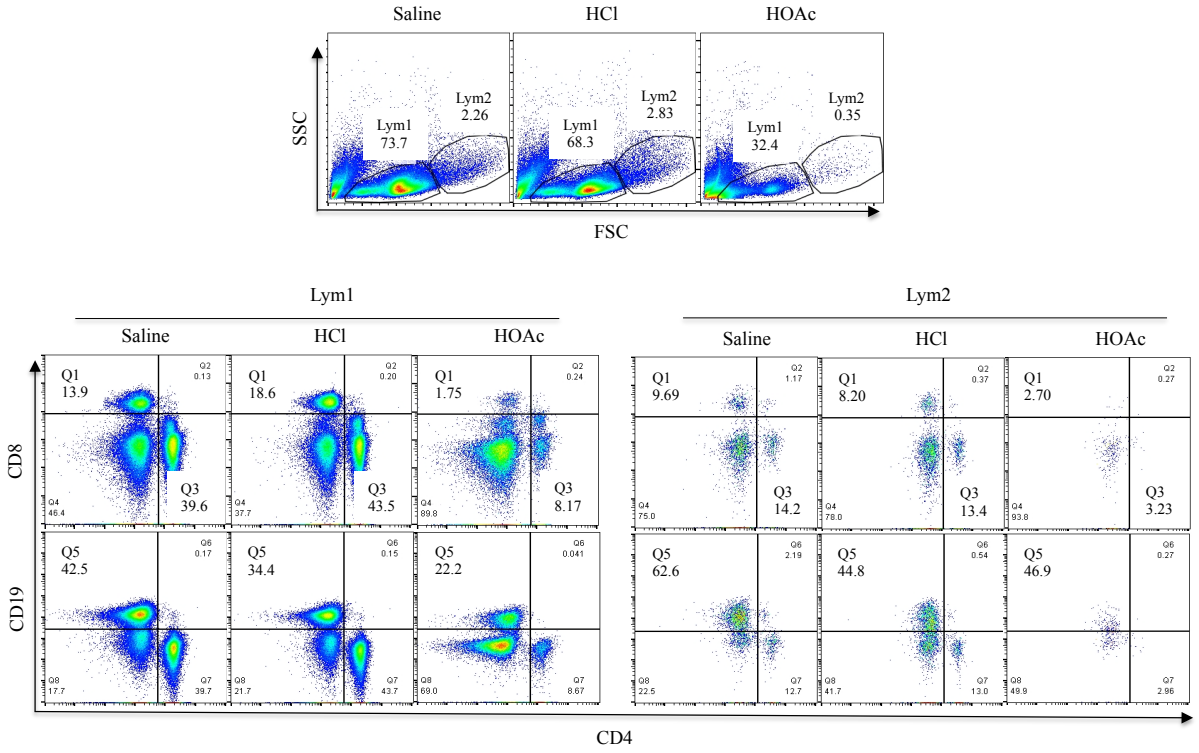

Fig. S1 (b) The upper panels show the Lym1 and Lym2 lymphocyte populations in the MLNs of the different treatment groups. The lower panels show the populations of CD4, CD8 T cells and B cells ($CD19^{+}$) in the Lym1 and Lym2 lymphocytes. Numbers in the plots are the percentages of each cell populations.

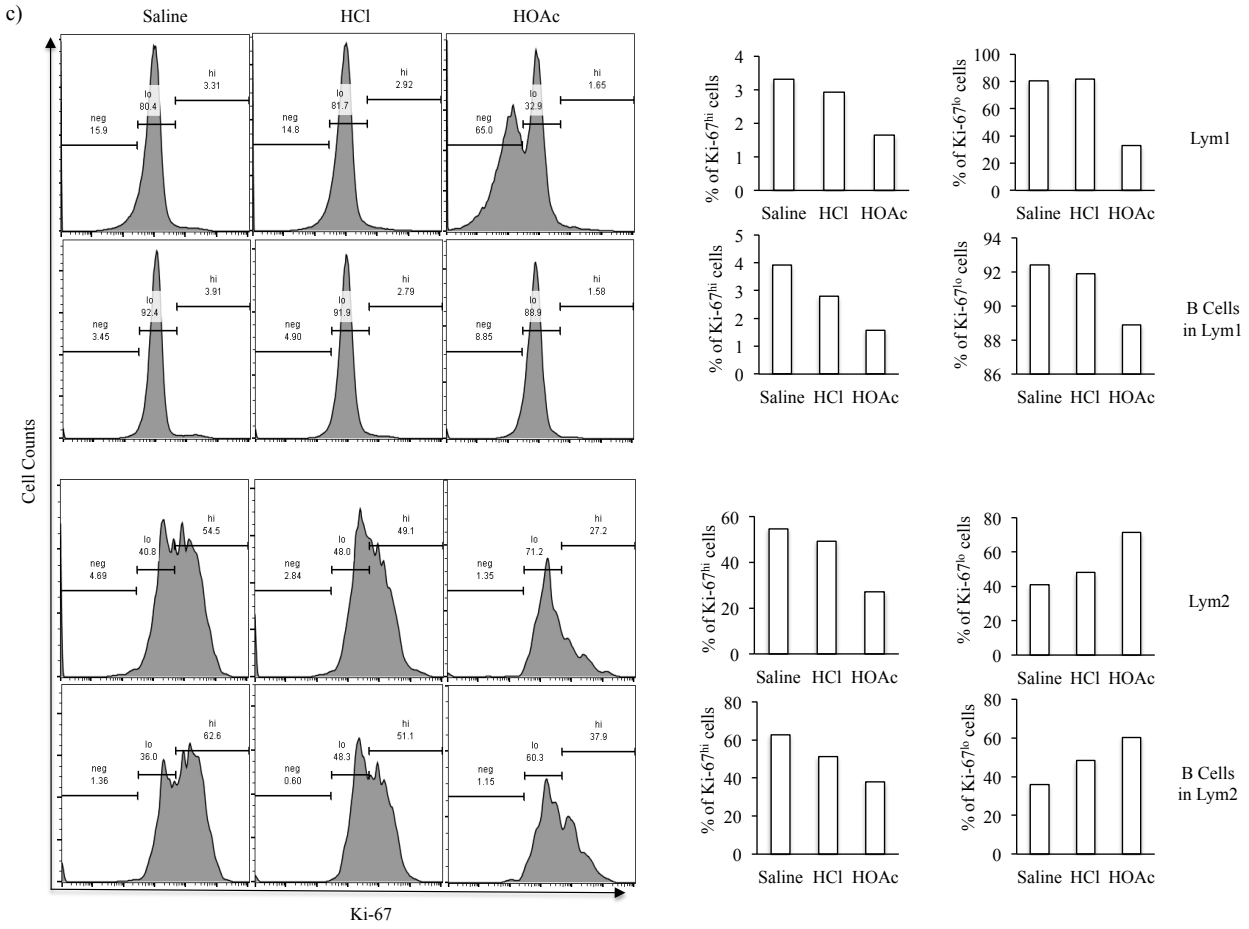

Fig. S1 (c) Expression of Ki-67. Left panels are histograms showing Ki-67 expression, and percentages of Ki-67 high, low, and negative cells in Lym1, Lym2 and the B cells thereof. Right panels are graphic presentation of the percentages of the Ki-67 high and low cells.

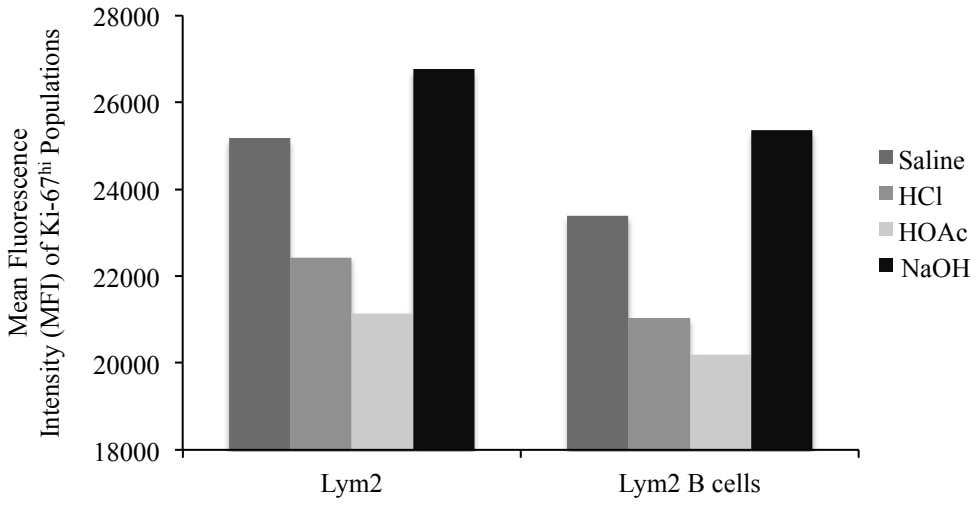

Fig. S2 Mean fluorescence intensities of Ki-67^{hi} cells in the Lym2 populations and their B cells of the different treatment groups in Figure 4c.

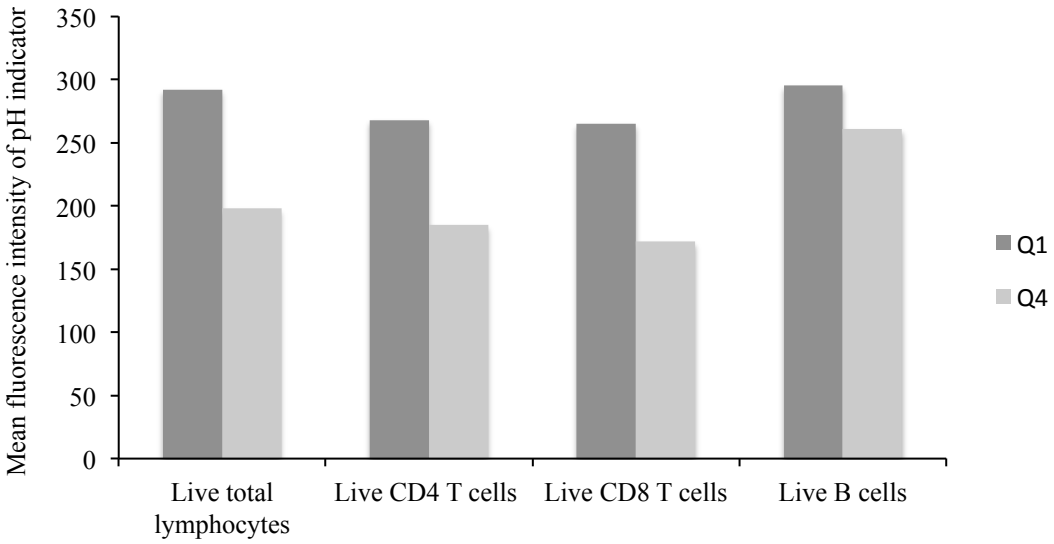

Fig. S3. Bar graph showing the mean fluorescence intensities (MFI) of the pH indicator of the early apoptotic (Annexin V^{hi}) cells in quadrant 1 (Q1) and the non-apoptotic (Annexin V^{lo}) cells in quadrant 4 (Q4) in Figure 5d. Higher MFI indicates lower pH.

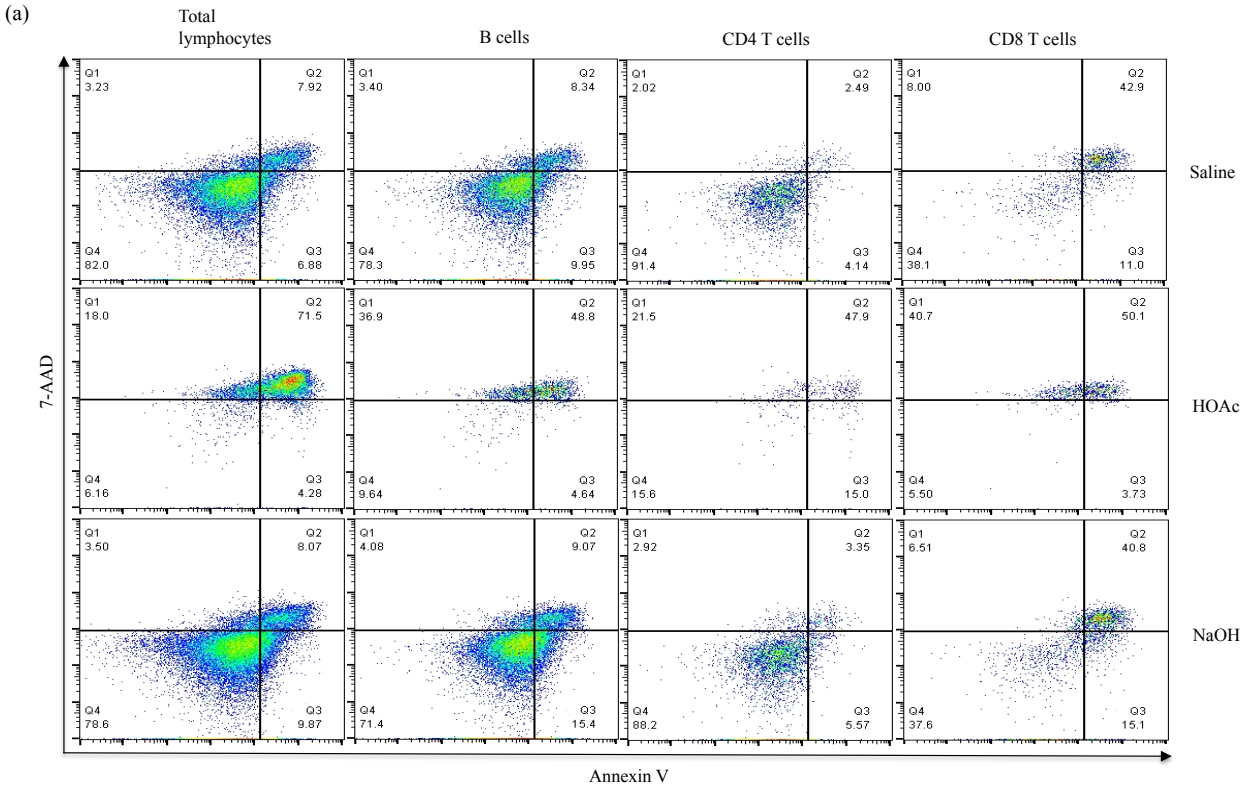

Fig. S4. Induction of apoptosis of in vitro cultured lymphocytes by low intracellular pH. After mitogenic stimulation, the cells were treated with saline or saline plus HOAc or NaOH in FBS, then stained with then intracellular pH indicator pHrodo^{TM} Green, Annexin V, and 7-AAD.

(a, b) Lymphocytes stimulated with anti-CD3 plus IL-2.

(a) Induction of apoptosis by acid treatments of anti-CD3 plus IL-2-stimulated lymphocytes. Shown are pseudocolor plots of Annexin V and 7AAD staining of the different lymphocyte populations in the different treatment groups.

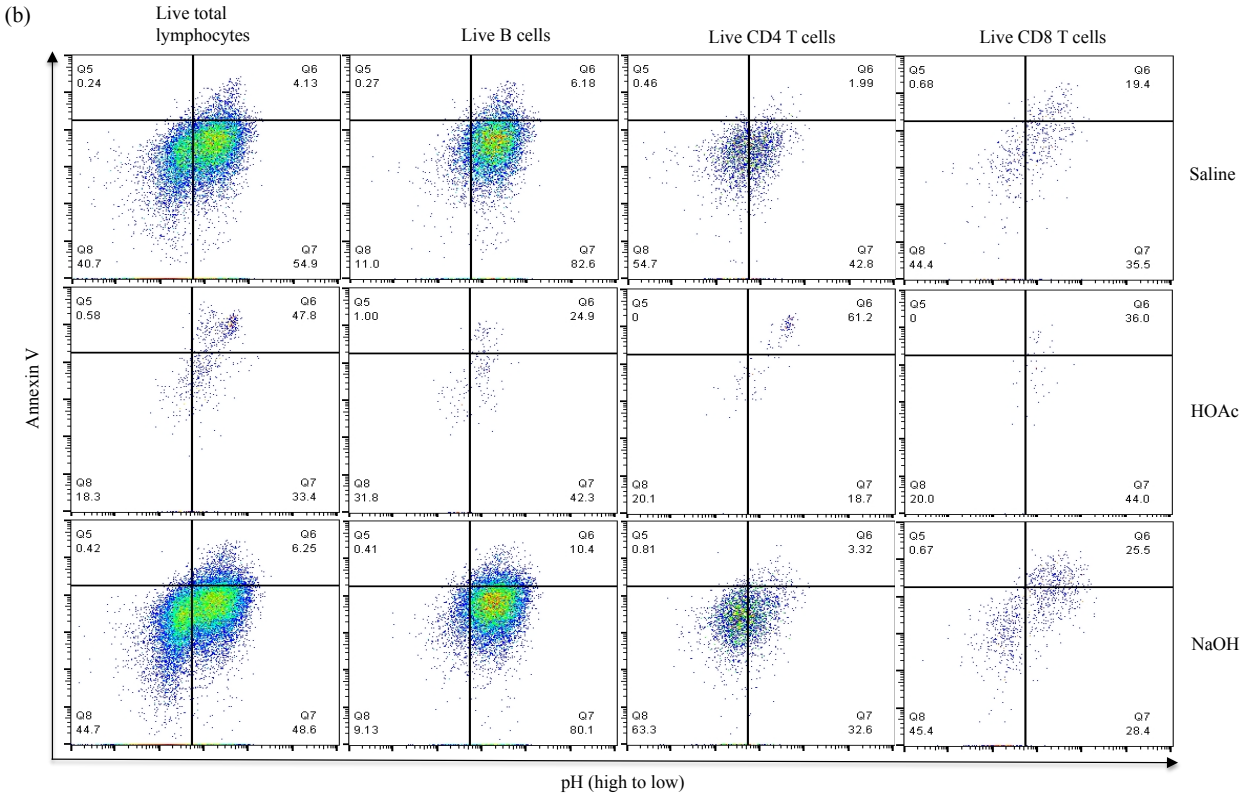

Fig. S4 (b) Low intracellular pH in early apoptotic cells of the anti-CD3 plus IL-2-stimulated lymphocytes. Shown are pseudocolor plots of the pH indicator and Annexin V staining in the indicated live (7AAD$^-$) lymphocyte populations in the different treatment groups.

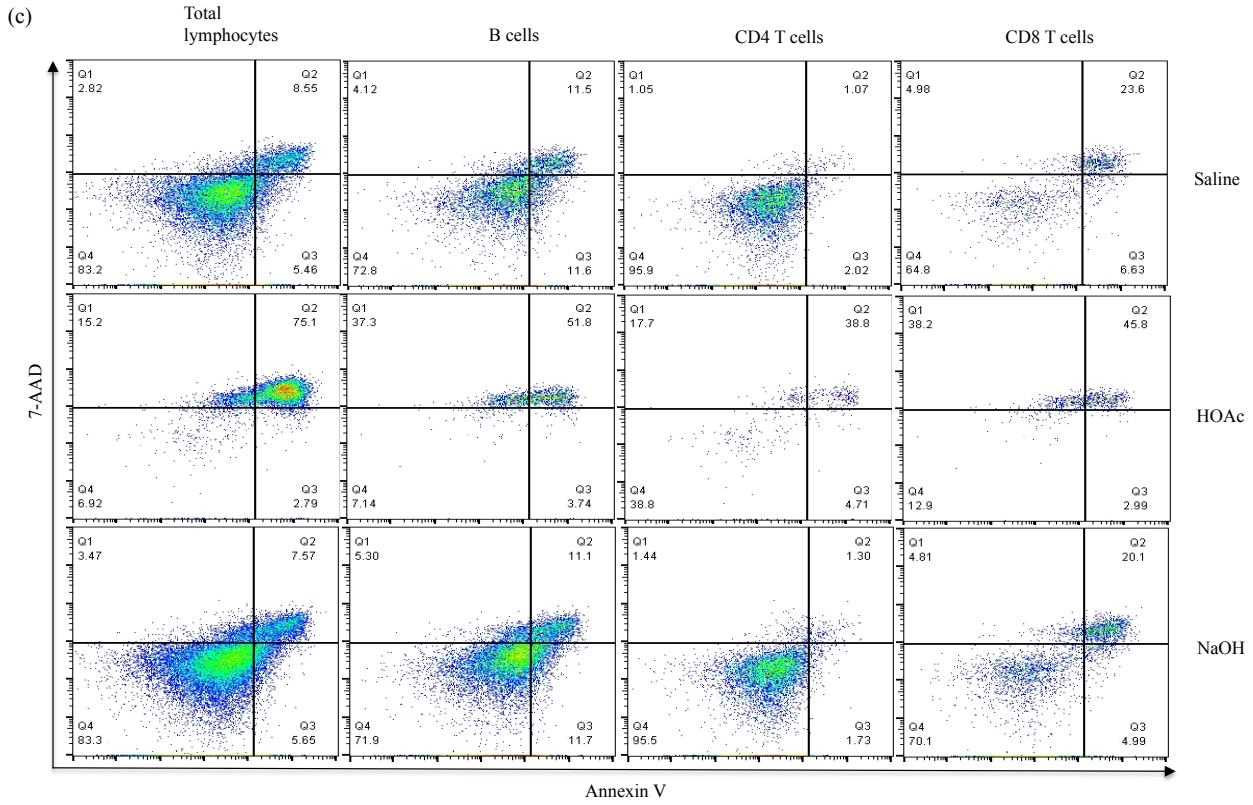

Fig. S4 (c, d) Lymphocytes stimulated with LPS plus IL-4.

(c) Induction of apoptosis by acid treatments of LPS plus IL-4-stimulated lymphocytes. Shown are pseudocolor plots of Annexin V and 7AAD staining in the different lymphocyte populations of the different treatment groups.

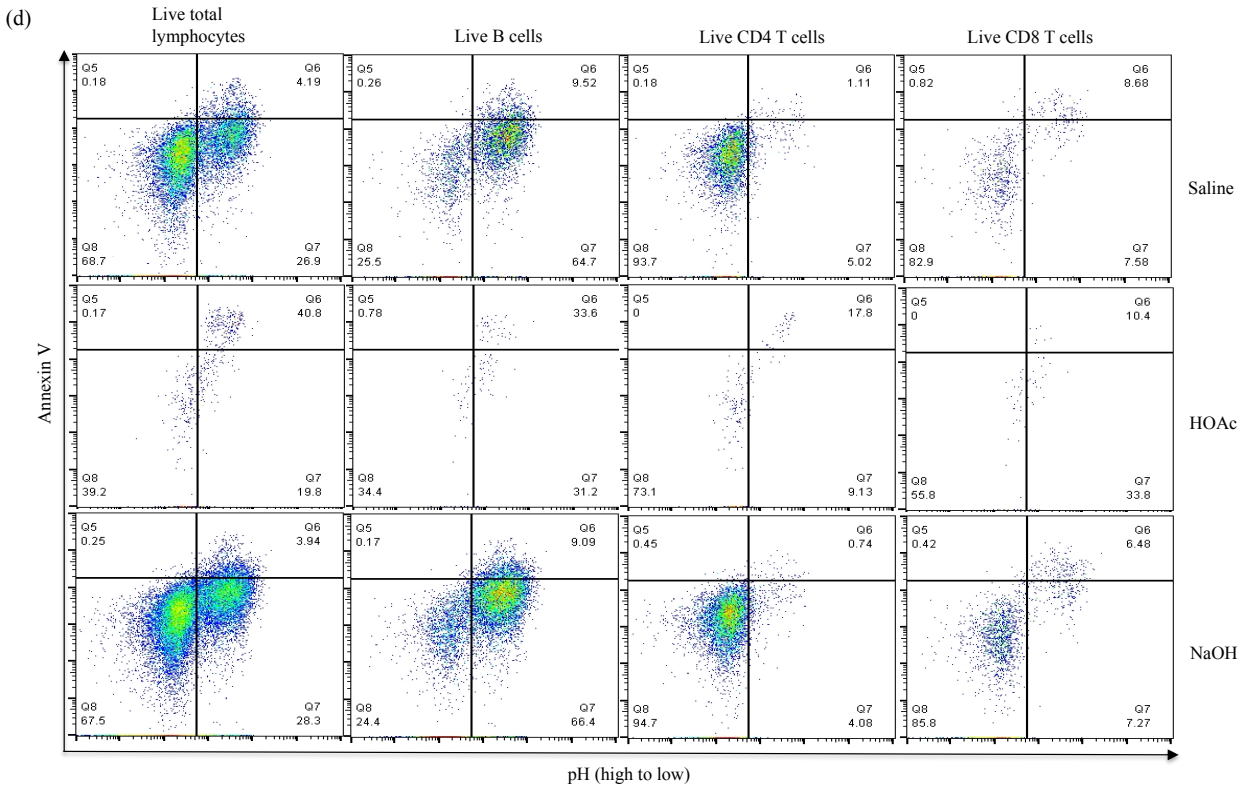

Fig. S4 (d) Low intracellular pH in early apoptotic cells of LPS plus IL-4-stimulated lymphocytes. Shown are pseudocolar plots of the pH indicator and Annexin V staining in the live ($7AAD^-$) lymphocyte populations of the different treatment groups.

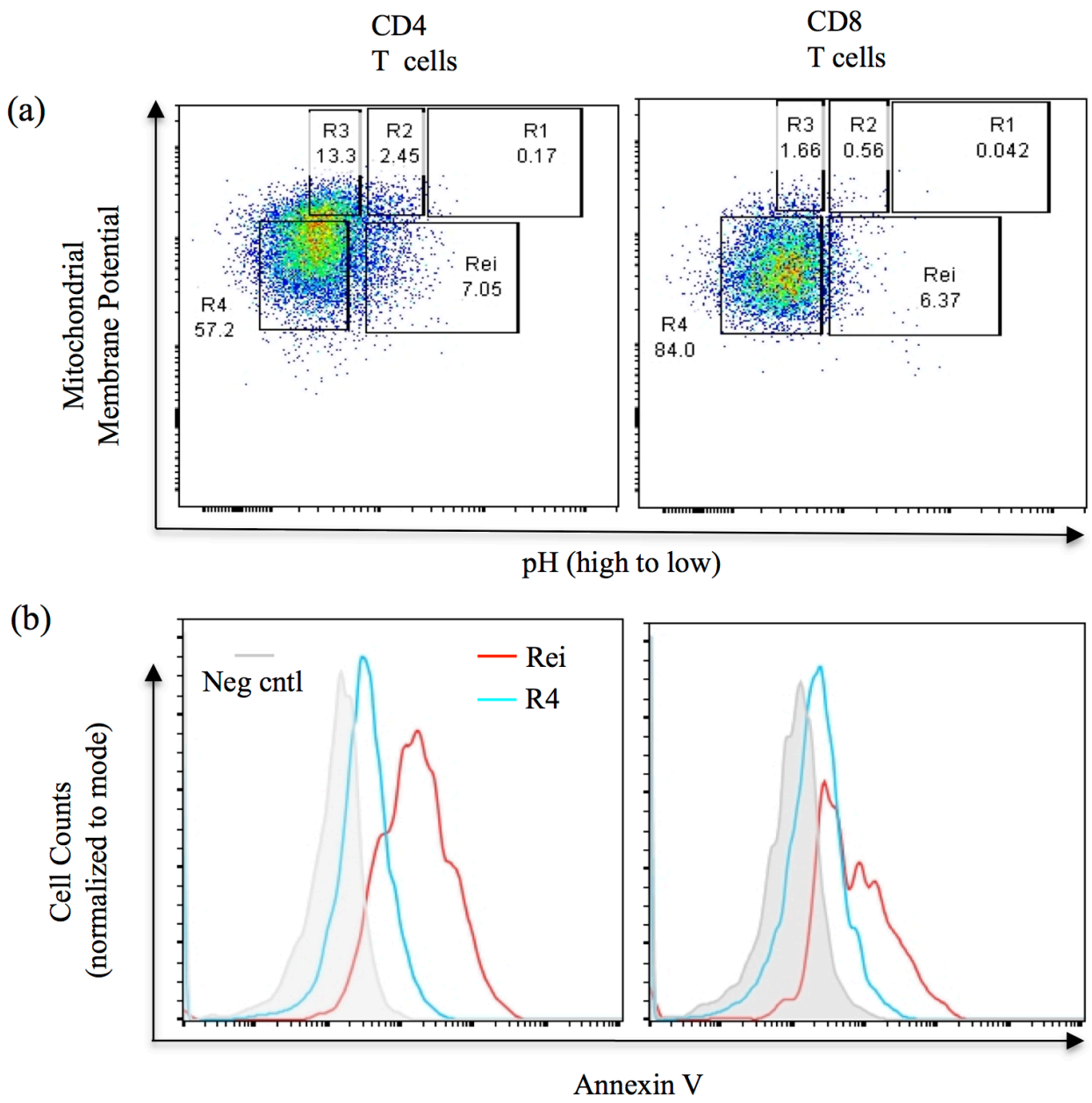

Fig. S5. Relations between intracellular pH and apoptosis in cells with low or ultralow mitochondrial membrane potentials. OVA sensitized mice were challenged with OVA on day 0 and 1, and MLNs were harvested on day 3. MLN cells were stained with MitoSpy and the pH indicator. Flow cytometric analyses of live CD4 and CD8 T cells are shown.

(a) Pseudocolor plots of MitoSpy and the pH indicator, showing the mitochondrial energy sufficient cell populations (R1 to R4), and mitochondrial energy insufficient (Rei) populations. Numbers in each gated region are the percentages of cells in the region.

(b) Overlaid histograms showing Annexin V staining of the Rei and R4 populations

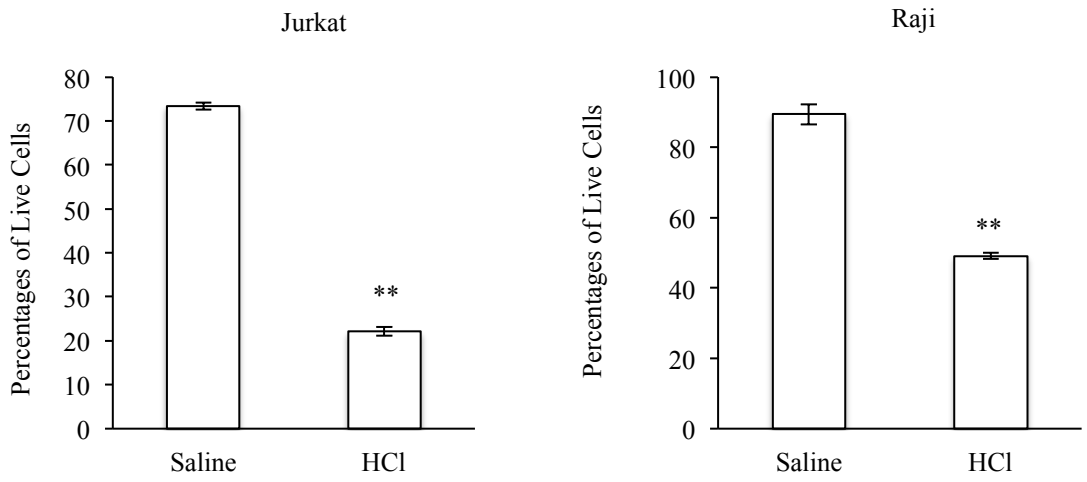

Fig. S6. Comparisons of tumor cell viabilities after treatment with saline or saline plus HCl in FBS. Shown are average viabilities of Jurkat and Raji cells determined by Trypan Blue staining in the different treatment groups as indicated. Error bars are standard deviations (3 replicates per treatment). Statistical significance of differences between the saline and HCl treatment groups was determined by Student t test, ** $p < 0.01$.